Postsynaptic plasticity of cholinergic synapses underlies the induction and expression of appetitive memories in *Drosophila*

Carlotta Pribbenow[1], Yi-chun Chen[1,*], Michael-Marcel Heim[1,*], Desiree Laber[1,*], Silas Reubold[1,*], Eric Reynolds[1,*], Isabella Balles[1], Raquel Suárez Grimalt[1,2], Carolin Rauch[1], Jörg Rösner[4], Gregor Lichtner[1,5], Sridhar R. Jagannathan[1], Tania Fernández-d.V. Alquicira[1], David Owald[1-3,+]

[1]Institute of Neurophysiology, Charité – Universitätsmedizin Berlin, corporate member of Freie Universität Berlin and Humboldt-Universität zu Berlin, and Berlin Institute of Health, Charitéplatz 1, 10117 Berlin, Germany

[2]Einstein Center for Neurosciences Berlin, Charitéplatz 1, 10117 Berlin

[3]NeuroCure, Charité – Universitätsmedizin Berlin, corporate member of Freie Universität Berlin and Humboldt-Universität zu Berlin, and Berlin Institute of Health, Charitéplatz 1, 10117 Berlin, Germany

[4]NWFZ, Charité – Universitätsmedizin Berlin, corporate member of Freie Universität Berlin and Humboldt-Universität zu Berlin, and Berlin Institute of Health, Charitéplatz 1, 10117 Berlin, Germany

[5]Universitätsmedizin Greifswald, Department of Anesthesia, Critical Care, Emergency and Pain Medicine, Ferdinand-Sauerbruch-Straße, 17475 Greifswald, Germany

* equal contribution, in alphabetical order

+correspondence: david.owald@charite.de

In vertebrates, several forms of memory-relevant synaptic plasticity involve postsynaptic rearrangements of glutamate receptors. In contrast, previous work indicates that *Drosophila* and other invertebrates store memories using presynaptic plasticity of cholinergic synapses. Here, we provide evidence for postsynaptic plasticity at cholinergic output synapses from the *Drosophila* mushroom bodies (MBs). We find that the nicotinic acetylcholine receptor (nAChR) subunit α5 is required within specific MB output neurons (MBONs) for appetitive memory induction, but is dispensable for aversive memories. In addition, nAChR α2 subunits mediate memory expression and likely functions downstream of α5 and the postsynaptic scaffold protein Dlg. We show that postsynaptic plasticity traces can be induced independently of the presynapse, and that *in vivo* dynamics of α2 nAChR subunits are changed both in the context of associative and non-associative memory formation, underlying different plasticity rules. Therefore, regardless of neurotransmitter identity, key principles of postsynaptic plasticity support memory storage across phyla.

Keywords: learning and memory; postsynaptic plasticity; cholinergic synapses; *Drosophila;* mushroom bodies

Introduction

Changing the strength of defined chemical synaptic connections within associative networks is widely believed to be the basis of memory storage[1–3]. However, it is unclear and frequently debated to what degree underlying neurophysiological and molecular mechanisms are evolutionarily conserved. One main difference between vertebrates and invertebrates is that memory-storing synapses in vertebrates use glutamate as their primary transmitter, while those in invertebrates (at least for *Drosophila melanogaster* and *Sepia officinalis*) use acetylcholine[4–6]. Furthermore, it is widely established that invertebrate nervous systems utilize presynaptic plasticity for storing memories, while the degree to which postsynaptic plasticity can be used is largely unclear. In contrast, it is well established that storing information in vertebrates can depend on both pre- and postsynaptic mechanisms, including postsynaptic rearrangements of neurotransmitter receptors.

Detailed knowledge of the anatomical wiring and functional signaling logic of the *Drosophila* learning and memory centers, the mushroom bodies (MBs)[5,7–21], allows one to address whether, despite the use of different neurotransmitter systems, memory storage modes are functionally comparable or evolutionarily conserved. The weights of Kenyon cells (KCs) to MB output neuron (MBON) synapses are modulated by dopaminergic neurons (DANs), which anatomically divide the MBs into at least 15 functional compartments, where information is stored on appetitive and aversive associations, in addition to non-associative learning such as the relative familiarity of an odor[5,7-12,15,22,23].

Studies so far have identified several traits pointing towards presynaptic storage mechanisms within the KCs during memory formation[24–27]. Indeed, studies that have blocked neurotransmitter release from KCs during learning[28–31] have brought postsynaptic contributions to synaptic plasticity into question.

In vertebrates, typically, postsynaptic long-term changes[2,32,33] are mediated via NMDA-sensitive glutamate receptors (NMDAR) that induce ('induction'[3]) an expression phase ('expression'[3]) through changed glutamatergic AMPA receptor (AMPAR) dynamics in dependence of postsynaptic scaffolds like PSD-95[34]. Invertebrate nAChRs in principle could take over similar functions to their glutamatergic counterparts in vertebrates, despite their differing molecular characteristics[35]. Indeed, nAChRs are pentamers that can be composed of homomeric assemblies of α subunits or heteromeric combinations of different α and β subunits. The composition of subunits determines the physiological properties of the nAChRs[35–38], and synaptic weights could, in theory, be adjusted through the exchange of receptor subunits or entire complexes.

Here, we capitalize on the genetic accessibility to individual output neurons of the MBs to directly test whether postsynaptic receptors play a role in memory storage. Derived from combined neurophysiological, behavioral, light microscopic and molecular approaches, our data are supportive of a sequential role for nAChR subunits in appetitive memory storage at the level of MBONs. Using artificial training protocols, we demonstrate that postsynaptic calcium transients can change in response to concurrent activation of dopaminergic neurons and application of acetylcholine, circumventing KC output. Blocking KC output during appetitive, but not aversive, learning abolishes memory performance. Moreover, specific knock-down of the α5

106 nAChR subunit, but none of the other six α subunits, in the M4/6 MBONs (also known
107 as MBON-γ5β'2a, MBON-β'2mp, MBON- β2β'2a and MBON-β'2mp bilateral) – an
108 output junction involved in coding appetitive and aversive memories[7,11,17] – impairs
109 immediate appetitive memories. Knock-down of α2 or α5, however, interferes with 3-
110 hour appetitive memories, as does knock-down of the scaffold Discs large (Dlg). We
111 report differential distribution of α subunits throughout the MB and demonstrate that
112 signal recovery of GFP-tagged subunits (as measured through fluorescence signal
113 recovered after photobleaching) is changed through plasticity protocols. In addition,
114 postsynaptically expressed non-associative familiarity learning also depends on α5
115 and α2 signaling as well as α2 dynamics. We propose a temporal receptor model and
116 speculate that, in *Drosophila*, nAChR subunits α5 and α2 take roles similar to NMDA
117 and AMPA receptors in vertebrates for memory induction and expression, indicating
118 that the general principle for postsynaptic plasticity independent of the
119 neurotransmitter system used, could be conserved throughout evolution.
120

121 ## Results

122

123 ***Neurotransmitter release from Kenyon cells is required for appetitive learning***

124

125 One key argument in favor of exclusively presynaptic memory storage
126 mechanisms in *Drosophila* is based on experiments suggesting that blocking KC or
127 KC subset output selectively during learning leads to unaltered or mildly changed
128 memory performance[28–31]. If the postsynapse need not see the neurotransmitter during
129 training, it would likely be dispensable for memory induction. We revisited such
130 experiments and blocked KC output during T-maze training, exposing the animals
131 either to sugar-odor or shock-odor pairings (Fig. 1 a-b, Supplementary Fig. 1a-b).
132

133 We expressed the temperature-sensitive Dynamin mutant UAS-*Shibire*^{TS} (Shi)
134 at the level of KCs, trained animals at the restrictive temperature, and tested for
135 memory performance at permissive temperature 30 minutes later. These
136 manipulations allowed us to interfere with the synaptic vesicle exo-endocycle
137 specifically during conditioning, while reinstating neurotransmission afterwards.
138 Consistent with previous reports[28,30,31], a slight drop in aversive memory performance
139 (Fig. 1a) was not statistically different from their genetic controls, and also observable
140 in the permissive temperature controls (see Supplementary Fig. 1a). In contrast,

141 memories were completely abolished following block of KC output during appetitive
142 training (Fig. 1b, Supplementary Fig. 1b).
143
144 We next asked whether the requirement for neurotransmission during
145 appetitive learning was specific to the KC output synapse. To do so, we took an
146 analogous approach, this time blocking neurotransmission from downstream M4/6
147 (MBON-γ5β'2a, MBON-β'2mp, MBON- β2β'2a and MBON-β'2mp bilateral) MBONs
148 during appetitive training. We focused on the M4/6 set of MBONs as blocking these
149 during memory retrieval crucially interferes with appetitive memory expression, while,
150 on a physiological level, memory-related plasticity is observable[5,7,13]. When blocking
151 M4/6 during appetitive training, but not retrieval, memory scores were similar to those
152 of control groups (Fig. 1c), suggesting that the sites of plasticity are likely to be the KC
153 to MBON synapse in general, with one major site specifically being the connections
154 between KCs and M4/6 MBONs.
155
156 Thus, our experiments suggest that neurotransmitter release from KCs during
157 training is required for the formation of appetitive memories, but is less crucial for the
158 formation of aversive memories.
159
160
161 ***The α5 nAChR subunit is required for induction, and α2 for expression of***
162 ***appetitive memories***
163
164 Requirement for presynaptic neurotransmitter release alone does not
165 necessarily mean that postsynaptic plasticity is involved in appetitive memory
166 formation. To address a putative role for postsynaptic sensitivity in memory formation,
167 we next interfered with the postsynaptic receptor composition. Given that KCs are
168 cholinergic, we screened for memory requirement of all nicotinic α-subunits at the level
169 of the M4/6 MBONs (Fig. 2) using previously published[4, 51] genetically-targeted RNAi.
170 We concentrated on the nAChR α subunits, as they are crucial components for all
171 possible heteromeric or homomeric receptor pentamers[36].
172
173 When flies were tested for immediate appetitive memory, only knock-down of
174 the α5 subunit produced performance that was statistically different from the controls
175 (Fig. 2a, Supplementary Fig. 2a,i). Testing 3-hour appetitive memory performance
176 revealed a significant memory impairment in flies with α5, α1 and α2 knock-down (Fig.

177 2b, Supplementary Fig. 2b,j-l). While α5 subunits can form homomeric channels[38], α1
178 and α2 can partake in heteromeric channels together[37]. We therefore concentrated on
179 the α5 and α2 nAChR subunits in subsequent analyses.
180
181 To exclude developmental contributions to the observed memory defects, we
182 repeated the immediate and 3-hour appetitive memory experiments for α5 as well as
183 the 3-hour appetitive memory experiments for α2 knock-down animals, while
184 suppressing RNAi expression using the temperature-sensitive Gal4 repressor Gal80^{ts}
185 during development, up until 3-5 days before memory testing. Memory impairments
186 were confirmed in all cases (Fig. 2e-g), but not detected in temperature controls
187 (Supplementary Fig. 2e-g).
188
189 We also tested aversive immediate and 3-hour memory using the same genetic
190 settings (Fig. 2c,d, Supplementary Fig. 2c,d). None of the knock-downs differed
191 significantly from controls, with the exception of α7 at the 3-hour time point. As,
192 comparable to vertebrate systems, α7 also plays a significant role at presynaptic
193 neurites[39], we did not follow up on this observation in this study.
194
195 As M4/6 output is also required for appropriate aversive memory expression[7,11],
196 α2 and α5 knock-down not impacting aversive memory performance suggested that
197 the observed appetitive memory impairments were not simply a consequence of lost
198 postsynaptic sensitivity to acetylcholine. To further corroborate this, we turned to a
199 brain explant preparation and applied acetylcholine focally to the dendrites of M4/6
200 neurons that expressed the calcium indicator GCamp6f, for both control and knock-
201 down settings, in the presence of the blocker of voltage-gated sodium channels
202 TTX[4,40]. Dendritic calcium transients were comparable between all groups
203 (Supplementary Fig. 3e). We also observed presynaptic sensitivity in all genotypes
204 (*not shown*) after applying acetylcholine to the presynaptic MBON boutons, making
205 presynaptic deficits following α2 or α5 knock-down unlikely.
206
207 Therefore, we conclude that, at the level of M4/6 neurons, immediate and 3-
208 hour appetitive memories are affected by knock-down of the α5 subunit, whereas 3-
209 hour memories also require the presence of α1- and α2-bearing receptors in addition.
210 The observed temporal profile of requirement for memory of α1- and α2-bearing
211 receptors relative to those incorporating the α5 subunit, could potentially point to a

212 temporal sequence of receptor function during initial memory formation and
213 subsequent memory expression.
214
215
216 ***The postsynaptic scaffold Dlg is required for 3-hour appetitive memory***
217
218 At mammalian glutamatergic synapses postsynaptic receptor-mediated
219 changes in synaptic weight rely on receptor stabilization or destabilization that can be
220 mediated via scaffolding molecules. One such scaffold, PSD-95, that is mostly involved
221 in AMPA receptor motility, is conserved at *Drosophila* synapses. The orthologue
222 Dlg[41,42] is expressed throughout the brain, with mushroom body compartment-specific
223 enrichment noted previously[43] (also compare Fig. 4a,b). We investigated appetitive
224 and aversive memory performance following M4/6-specific knock-down of Dlg (Fig. 2a-
225 d, Supplementary Fig. 2a-d). Performance scores comparable to controls were found
226 for both immediate appetitive and aversive memories (Fig. 2a,c, Supplementary Fig.
227 2). Dlg knock-down, however, specifically abolished 3-hour appetitive memory
228 performance (Fig. 2b,d, Supplementary Fig. S2b), while Gal80^{ts} experiments excluded
229 a developmental defect (Fig. 2h, Supplementary Fig. 2h). The temporal profile of Dlg
230 requirement therefore closely matched that of α2 nAChR subunits.
231
232
233 ***Bypassing the presynapse: induction of persistent associative plasticity in the***
234 ***postsynaptic compartment***
235
236 Recent ultrastructural data has revealed direct synaptic connections between
237 dopaminergic neurons and MBONs[23,44], giving rise to a motif that could allow for
238 postsynaptic plasticity induction (see schematic in Fig. 3a). In order to directly test
239 whether postsynaptic plasticity could take place at the level of MBONs, we next
240 conducted neurophysiological proof-of-principle experiments.
241
242 To minimize plasticity induced by acute sensory experiences or general
243 network activity, we used an explant brain preparation bathed in TTX from flies
244 expressing the red light-activatable channelrhodopsin CsChrimson in a subset of
245 dopaminergic neurons (PAM neurons; R58E02-LexA) and the calcium indicator
246 GCaMP6f in M4/6 MBONs.
247

248 While dopamine release was controlled by red light flashes, neurotransmitter
249 release from KCs was mimicked by focal pressure ejection of acetylcholine to the
250 dendrites of the M6 (MBON-γ5β'2a) MBON (M6 was chosen for technical reasons, as
251 these neurons are most accessible for the used imaging technique). We verified that
252 KC presynapses do not respond to acetylcholine application[4], using both calcium
253 imaging and imaging of synaptic vesicle exocytosis at the level of KC axons (Fig. 3c
254 and Supplementary Fig. 3f,g). The observed absence of KC activation, with
255 acetylcholine being applied from an external source (Fig. 3a), minimized noise
256 attributable to possible presynaptic contributions.
257
258 Our protocols consisted of training phases where we differentiated between
259 temporal pairing of acetylcholine and optogenetic activation of dopaminergic neurons
260 ('paired', Fig. 3b,h), dopamine only ('red-light only', Fig. 3b,e,g), or 'acetylcholine only'
261 (Fig. 3b,d,f). Acetylcholine application preceded (pre) and followed each training step
262 (post) to establish baseline responses and to assess synaptic weights following
263 training ('testing'). We found that test responses were significantly elevated following
264 the paired condition (Fig. 3h). This potentiation was not observed when testing after
265 acetylcholine only or dopamine only training (Fig. 3f,g). Importantly, we also did not
266 observe any changes when pairing acetylcholine application with red light in non-
267 CsChrimson-expressing controls (Supplementary Fig. 3c,d).
268
269 Because we are using global acetylcholine application instead of sparse
270 activation of single synapses, these experiments likely do not reflect *in vivo*
271 physiological settings[7]. However, our proof of principle experiments demonstrate that
272 postsynaptic sensitivity can change independently of the presynapse. Indeed, the
273 observed postsynaptic potentiation was not observed, when knocking-down α2 in M4/6
274 (Supplementary Fig. 3h), consistent with postsynaptic plasticity being linked to the
275 requirement of nicotinic receptors in memory storage.
276
277 ***Non-uniform distribution of nAChR α-subunits throughout MB compartments***
278
279 Our data so far are suggestive of α2-containing nicotinic receptors being
280 involved in appetitive memory storage. To test whether receptor levels were
281 interdependent, we made use of a newly established CRISPR-based genomic
282 collection of GFP-tagged endogenous nAChR subunits (Woitkuhn, Pribbenow,
283 Matkovic, Sigrist and Owald, *unpublished*) covering all α subunits (with the exception

of α3) under control of their endogenous promoter, allowing for analyses of receptor distribution and dynamics in a dense neuropile *in situ*.

We first characterized receptor subunit signals throughout the 15 MB compartments, several of which have been shown to be involved in the encoding of specific memories. We found a non-uniform distribution (Fig. 4a,b, Supplementary Fig. 4) that was unique for each subunit, indicating considerable heterogeneity of receptor composition.

α5, which is required for immediate and 3-hour appetitive memories, was abundant throughout the γ lobe, including γ5 (innervated by M6) and slightly less at the level of β'2 (innervated by M4 and in parts by M6). α2 subunits, required for 3-hour appetitive memories, showed similarly high relative abundance in β'2 and γ5 (Fig. 4a,b). Of note, these subunits were also detected in other MB output compartments, such as α'3, which harbors MBONs involved in non-associative familiarity learning[15].

We next evaluated, whether the fluorescent signals of the α2 and α5 subunits (with α5 potentially functioning upstream of α2, Fig. 2) observed in the β'2 and γ5 compartments were derived from receptors within the dendritic processes of M4/6. To do so, we performed cell-specific knock-down experiments using VT1211-Gal4 and quantified the relative fluorescent signal of the knock-down compartment relative to the neighboring unmanipulated compartments (Fig. 4c-f).

Knock-down of the α5 nAChR subunit reduced the relative $\alpha5^{GFP}$ signal specifically and significantly in γ5 and β'2 (Fig. 4e,f). α5 abundance was, however, unaltered when knocking-down α2 or Dlg, which is in line with α5 functioning as a possible trigger for plasticity processes.

Likewise, confirming that the observed signal was derived from M4/6 MBON dendrites, α2 knock-down reduced relative $\alpha2^{GFP}$ levels significantly throughout the β'2 and γ5 compartments (Fig. 4c,d). Strikingly, we also observed reduced α2 nAChR subunit levels following α5 subunit knock-down in the β'2 compartment or Dlg knock-down in the β'2 and γ5 compartments (Fig. 4c,d), which would be in line with a Dlg-dependent sequential requirement of receptor subunits during memory formation (also compare behavioral data in Fig. 2).

318 Our data therefore are consistent with a role of α5 nAChR subunits and Dlg
319 functioning upstream of α2 subunit-positive receptors, at least within the β'2
320 compartment.
321
322
323 ***nAChR subunits shape synaptic MB output properties***
324
325 We next focused on implications of α2 subunit knock-down on postsynaptic
326 function of M4/6 MBONs. Axonal calcium transients had previously been shown to be
327 decreased following knock-down of α subunits[4]. However, both increased or
328 decreased postsynaptic drive could lead to changed dendritic integration properties
329 underlying reduced signal propagation[45].
330
331 We expressed GCaMP6f in M4/6 MBONs (Fig. 5a), and exposed the flies
332 repeatedly to alternating puffs of the odors octanol (OCT) and MCH (Supplementary
333 Fig. 5a,b). We focused our experiments on the β'2 compartment (Fig. 5), as this is
334 innervated by M4 MBONs that show input-specific plasticity following appetitive
335 learning[7]. Initial dendritic odor responses were not statistically different between α2
336 subunit knock-down and controls (Fig. 5b,c), while initial odor-evoked dendritic calcium
337 transients were significantly elevated following knock-down of α5 (Fig. 5b,c).
338 Importantly, while control animals showed a relative facilitation in odor-specific calcium
339 transients after several exposures to OCT, we did not detect this in α2 knock-down
340 animals (Fig. 5d,e). Odor responses following α5 knock-down, however, clearly
341 depressed after multiple odor exposures (Fig. 5f), indicating that lack of α5 can lead to
342 pre-potentiated synaptic transmission, while α2 nAChR subunit knock-down interfered
343 with odor-evoked baseline transmission properties to a lesser extent. We did not
344 observe any changes in calcium signals at the level of the corresponding KC axons,
345 further supporting that the observed plasticity was of postsynaptic origin
346 (Supplementary Fig. 5h,i).
347
348 **The α2 *nAChR subunit is required for the formation of appetitive memory***
349 ***traces* in vivo**
350
351 Of note, the observed facilitation in M4/6 of controls was not apparent when
352 using repeated application of MCH, indicating that parameters underlying the observed
353 non-associative plasticity are odor-dependent (Supplementary Fig. 5e). However, the

354 only slight effects on base-line MCH-induced responses observed for α2 knock-down
355 animals, allowed us to next investigate the role of α2 during *in vivo* associative
356 appetitive learning.
357
358 We performed *in vivo* training under the microscope experiments using an
359 absolute paradigm, pairing odor (MCH) exposure with *ad libitum* sugar feeding during
360 training. Comparing odor responses at the level of M4 before and after training
361 revealed a marked depression for control animals in line with previous observations[7,17]
362 (Fig. 5g). Importantly, after MBON-specific knock-down of α2, this training-induced
363 plasticity was not observed (Fig. 5h).
364
365 Together, our data point towards a mechanism, where nicotinic receptor
366 subunits shape synaptic properties (Fig. 5), with α2 as a postsynaptic substrate
367 underlying appetitive training-induced plasticity processes.
368
369
370 **In vivo *imaging of postsynaptic receptor plasticity reveals altered α2 dynamics***
371
372 Structural changes at the level of the receptor composition are hallmarks of
373 postsynaptic plasticity expression in vertebrates. Typically, rearrangements can be
374 measured by altered dynamics (or motility) of receptors that can reflect incorporation
375 or removal of receptor complexes. We next sought to test whether dynamic receptor
376 behavior could serve as a structural correlate of cholinergic postsynaptic memory trace
377 expression. To do so, we turned to *in vivo* imaging experiments of the endogenously
378 tagged α2 subunit (Fig. 6, Supplementary Fig. 6). Flies were either tethered under the
379 two (Fig. 6) or the single photon confocal (Fig. 7) microscope and subjected to training
380 protocols. Endogenous *in situ* receptor dynamics at the level of the β'2 compartment
381 of the MB were estimated as fluorescence recovery after photobleaching (FRAP),
382 allowing us to also pick up small increases in signal (Fig. 6a-c).
383
384 We conducted artificial appetitive training protocols by exposing the tethered
385 animals to odor with or without simultaneous focal injection of dopamine to the β'2
386 compartment of the MB (Fig. 6a-c). We performed two different sets of protocols
387 comparing recovery of $\alpha2^{GFP}$ (Fig. 6b, Supplementary Fig. 6b).
388

389 Following photobleaching, individual flies were exposed to consecutive focal
390 injections of dopamine, odor, and odor paired with focal dopamine injection. MCH
391 induced significantly increased fluorescence recovery when compared to dopamine
392 injections only or odor paired with dopamine (Fig. 6d,e). Dopamine, therefore, does
393 not induce plasticity on its own, and further, it suppresses odor-induced recovery when
394 applied simultaneously with an odor. To rule out that recovery depended on the type
395 of odor used, we also conducted similar experiments using OCT, this time testing all
396 conditions in separate flies. After photobleaching, flies were either exposed to a focal
397 injection of dopamine, an odor stimulus, or odor paired with focal dopamine injection.
398 We only observed significant recovery in the odor only condition, whereas dopamine
399 and odor paired with dopamine induced no significant recovery (Supplementary Fig.
400 6a-d).
401
402 Thus, our data indicate that pairing odor presentation with dopamine
403 application stalls $\alpha2^{GFP}$ dynamics, potentially by either stabilizing the already present
404 amount of receptor or hindering new incorporation of α2-containing receptors.
405 Interestingly the opposite, increased receptor dynamics, is observed after odor
406 exposure without reinforcer. Note that the absence of acute stimuli (constant air stream
407 only), did not induce signal recovery, demonstrating that it is the presence of the odor
408 that changes baseline receptor behavior (Supplementary Fig. 6e). Thus, stalling α2
409 dynamics can be correlated to depression of M4/6 MBON synapses[7,13] following
410 appetitive training (Fig. 5g,h).
411
412
413 ***Familiarity learning alters postsynaptic receptor dynamics***
414
415 We next asked whether postsynaptic plasticity expressed through α5 and α2
416 subunit interplay could underlie other forms of learning represented in the MBs. We
417 turned to the α'3 compartment at the tip of the vertical MB lobe that has previously
418 been shown to mediate odor familiarity learning. This form of learning allows the animal
419 to adapt its behavioral responses to new odors and, importantly, permits for assaying
420 direct odor-related plasticity. Importantly, this compartment follows different plasticity
421 rules, because the odor serves as both the conditioned (activating KCs) and
422 unconditioned stimulus (activating corresponding dopaminergic neurons)[15]. While
423 allowing us to test whether the so far uncovered principles could also be utilized in a

424 different context, it also provides a less complex test bed to further investigate whether
425 α5 functions upstream of α2 dynamics.
426
427 Confirming previous observations[15], a repeated odor application paradigm (Fig.
428 7a) led to the depression of postsynaptic calcium transients at the level of the α'3
429 MBONs (Fig. 7b). Importantly, we did not detect a corresponding depression on the
430 presynaptic side when imaging arbors of a sparse α'β' KC driver line within α'3 (Fig.
431 7b), further indicating that memories were predominantly stored postsynaptically in this
432 compartment. We next performed *in vivo* FRAP experiments following familiarity
433 learning paradigms. After odor training, we observed clear recovery rates of $\alpha2^{GFP}$
434 signals compared to the control group, however not of $\alpha5^{GFP}$ or Dlg^{GFP} (Fig. 7 c-f,
435 Supplementary Fig. 7). Therefore, increased α2 subunit dynamics are triggered
436 through training events and, at the level of the α'3 compartment, accompany
437 postsynaptic depression of the MBONs.
438
439 To invariantly test whether the observed recovery was attributable to α2
440 expressed in α'3 MBONs, we trained animals while knocking-down α2 specifically in
441 α'3 MBONs. In accordance with the observed signal recovery deriving from MBONs,
442 no recovery was observed after α2 knock-down (Fig. 7g). Importantly, we did not
443 observe $\alpha2^{GFP}$ recovery when performing specific α5 knock-down in α'3 MBONs (Fig.
444 7g), indicating a role of α5 upstream of α2 also in this compartment.
445
446
447 ***α5 subunits govern induction and α2 subunits expression of non-associative***
448 ***familiarity learning***
449
450 Finally, we tested whether interfering with α5 and α2 nAChR subunits at the
451 level of α'3 MBONs would also impact familiarity learning behavior (Fig. 8).
452 Flies were covered in dust and subjected to repeated odor exposures[15]. As expected[15],
453 control flies readily groomed to remove the dust, however typically stopped this action
454 when detecting the novel odor (Fig. 8a-c). Over subsequent trials, control flies learned
455 that this odor was familiar and stopped reacting to the stimulus, continuing grooming
456 (Fig. 8a-c, Supplementary Fig. 8). Expressing RNAi to the α2 subunit at the level of the
457 α'3 MBONs clearly impacted learning: flies learned with decreased efficacy and only
458 after several trials (Fig. 8a-d). Strikingly, α5 RNAi-expressing flies failed to stop

459 grooming even to the first stimulus. Indeed, they acted as if they had already learned
460 that an odor was familiar (Fig. 8a-d).
461
462 Together, our data are in line with a model where α5 can induce memory
463 formation, while lack of α5 leads to fully potentiated synapses. Subsequent expression
464 of memory traces requires α2-containing receptors. Importantly, recovery
465 accompanies synaptic depression at the level of the α'3 MBONs, while being
466 suppressed by paired training in the β'2 compartment. Moreover, α2 appears to be
467 involved in both depression and facilitation of synapses. Thus, synapses could
468 bidirectionally utilize plasticity of the same receptor subunit for storing different types
469 of information (Fig. 9).
470
471
472 **Discussion**
473
474 Synaptic weight changes are widely recognized as substrates for memory
475 storage throughout the animal kingdom. How synapses adapt in order to change their
476 efficacy during learning has been a focus of attention over the last decades. While it is
477 undisputed that both pre- and postsynaptic mechanisms of memory storage exist in
478 vertebrates, invertebrate memory-related synaptic plasticity has been largely localized
479 to the presynaptic compartment, although some debates exist[1]. The core of the debate
480 boils down to a key question: do vertebrates and invertebrates use similar mechanisms
481 to store memories or are there fundamental differences? A first clear difference
482 appears to be the use of different neurotransmitter systems, glutamate and
483 acetylcholine respectively, in the vertebrate and *Drosophila* learning centers[4].
484
485
486 ***Postsynaptic plasticity in appetitive memory storage***
487
488 Here, we use the genetic tractability of the *Drosophila* system to directly
489 address postsynaptic plasticity during memory storage in invertebrates. Large
490 amounts of evidence from *Drosophila* so far suggests a presynaptic mode of memory
491 storage[24–28,46]. Moreover, it was demonstrated that block of KCs during learning does
492 not interfere with memory performance[28,30,31], although some studies blocking KC
493 subsets did find impairments[29,47] in the context of short-term appetitive memory. Lack

494 of necessity to detect neurotransmitter by the postsynapse in the course of memory
495 storage was interpreted as evidence for a presynaptic storage mechanism. If the
496 receptor does not 'see' the signal, it is dispensable for 'interpreting' it. Here, we
497 revisited such experiments and found, in accordance with previous studies, only mild,
498 if any, requirement for aversive memory storage. We, however, fully abolished
499 appetitive memories (Fig. 1) by blocking KC output during acquisition, providing a
500 model for postsynaptic plasticity (Fig. 9) that is induced and expressed through distinct
501 nAChR subunits (Fig. 2-8).
502
503 Our study hints towards different pre- and postsynaptic storage mechanisms
504 underlying aversive and appetitive memories. It also argues against the assumption
505 that appetitive and aversive memories will necessarily use the same molecular
506 machinery to store information. Findings in the past, predominantly based on
507 investigating aversive memories, have been generalized to learning per se. Indeed,
508 postsynaptic contributions have been ruled out for a synaptic junction required for
509 storage of aversive but not appetitive memories, which is fully consistent with our
510 findings[22]. Interestingly, arguing for a division of appetitive and aversive storage sites,
511 subpopulations of KCs have been implicated in aversive and appetitive memory
512 respectively[48]. Lastly, we do not wish to exclude a potential involvement of
513 postsynaptic plasticity in aversive memory formation per se. On the contrary, it is
514 conceivable that aversive memories also could have an appetitive component (release
515 from punishment). However, our experiments suggest that these influences are not as
516 crucial as for appetitive memories, at least in the context of single trial differential
517 associative learning.
518
519
520 ***Postsynaptic plasticity at the KC to MBON synapse***
521
522 Recent anatomical studies[23,44] have reported both dopaminergic innervation of
523 presynaptic KC compartments as well as somewhat unexpectedly direct synapses
524 between presynaptic dopaminergic terminals and MBONs. We devised an experiment
525 where we substituted KC input to the postsynaptic MBON compartment through
526 artificial acetylcholine injection, while rendering dopaminergic neurons switchable
527 through optogenetics. A protocol that trained and subsequently tested the synaptic
528 junction between KCs and MBONs, demonstrates that plasticity (represented by a
529 change in calcium responses to acetylcholine injection) was inducible by pairing

530 dopaminergic with postsynaptic MBON activation that lasted beyond the training stage
531 and was observable by mere 'recall-like' activation of the system (Fig. 3).
532
533 Our proof-of-principle experiments uncovered the ability to potentiate after
534 pairing M6 MBON activation and stimulating a broad population of dopaminergic
535 neurons that convey information on sugar, water or the relative valence of aversive
536 stimuli[5], while we find postsynaptic plasticity to be required for appetitive memory
537 performance (Fig. 3). However, previous studies looking into 'natural' appetitive sugar
538 conditioning uncovered a relative depression in M4 (another MBON of the M4/6
539 cluster) dendrites, when comparing the responses of the paired (CS+) and unpaired
540 odor (CS-) one hour after appetitive conditioning[5,7,13]. Moreover, we here show that *in*
541 *vivo* appetitive absolute training depresses subsequent responses to the trained odor
542 (Fig. 5). It is important to note that, here (Fig. 3), for our *in vitro* experiments, we
543 perform global activation of the postsynaptic compartment and not the natural typical
544 coverage of 5 % of input synapses per odor[49] (that allow for differential conditioning).
545 Induced changes are therefore likely not comparable to the natural settings, where
546 sparse sets of KCs and dopaminergic neurons are active within a tight temporal
547 window. Moreover, we here abolish network contributions (by suppressing active
548 signal propagation), to be able to concentrate on synaptic mechanisms during plasticity
549 induction. Thus, our artificial training (Fig. 3) through global dendritic activation likely
550 does not mirror precise physiological conditions allowing for plasticity of a sparse set
551 of synapses to convey odor-specificity to a memory, and should therefore only be
552 viewed as a proof of principle for postsynaptic plasticity induction per se. However, the
553 relatively small amplitude of potentiation observed actually fits previous[7] *in vivo*
554 observations. Importantly, because we are using TTX and local training of KC to M6
555 synapses in our experiments, we are furthermore missing additional disinhibition that
556 *in vivo* is mediated via the GABAergic MVP2 MBON[13,19]. Of note, similar protocols[50]
557 that involved broad activation of KCs (and thus did not circumvent the presynaptic
558 compartment) have demonstrated comparable plasticity induction at this synaptic
559 junction.
560
561 Local acetylcholine application to the MB can also activate calcium transients
562 in dopaminergic presynaptic terminals[51]. Therefore, our protocol could in principle
563 include some dopaminergic contributions already at baseline level. However, control
564 experiments using the paired training protocol in the absence of CsChrimson
565 expression in dopaminergic neurons, do not show any signs of plasticity (Fig. 3 and
566 Supplementary Fig. 3). Moreover, it has been previously demonstrated that, to actually

567 release dopamine from the presynaptic terminal, a coincident signal via carbon
568 monoxide is required[52,53]. Therefore, an unwanted activation of dopaminergic neurons
569 in our experiments is unlikely.
570
571 It should also be noted that M4, which shows depression (Fig. 5), and M6 have
572 common but also distinct physiological roles, for instance during aversive memory
573 extinction[13]. Besides that, different temporal requirements for M4 and M6 memory
574 expression have been reported[11]. It is therefore possible that physiological changes in
575 the context of appetitive learning led to different plasticity profiles in M4 and M6
576 neurons respectively, or that initial potentiation over time can be reverted to
577 depression. As noted above, MBON drive is bidirectionally modifiable and has the
578 propensity to both potentiate and depress[7,11,17,26].
579
580 We did not observe plasticity after paired training following α2 knockdown *ex*
581 *vivo* (Supplementary Fig. 3). In line with that, our *in vivo* experiments directly establish
582 a connection between learning-triggered synaptic plasticity and the α2 subunit (Fig. 5).
583 Appetitive training induced synaptic depression at the level of the β'2-MBON dendrites
584 of control animals. In animals where we concurrently knock-down α2 in M4/6 MBONs,
585 this synaptic depression, however, was not observable.
586
587
588 ***Nicotinic receptors could follow temporal sequence***
589
590 Lasting plasticity traces as observed here (Fig. 3) appear to fit the core criteria
591 for long-term potentiation of vertebrate glutamatergic postsynapses[3,54]. Plasticity can
592 be divided into an 'induction'[3] period mediated via NMDA receptors and a subsequent
593 'expression'[3] period that requires altered AMPA receptor dynamics[3]. Our findings here
594 lead to a model, where the nicotinic α5 subunit is required for the induction of appetitive
595 memories at *Drosophila* MBONs (Fig. 2, 9). We propose that α5 nAChR subunits (that
596 can form homomeric channels[38,39]) could take on a similar role to NMDARs. α5 would
597 gate the potentiation or depression of synaptic strength influencing the incorporation
598 or exchange of additional receptor subunits or complexes. In line with this, we show
599 that knock-down of α5 subunits interferes with familiarity learning in the α'3
600 compartment of the MBs: flies no longer form familiarity memories, they react to a novel
601 odor the same way as to a familiar one, 'as if they had learned that this new odor was
602 familiar before' (Fig. 7, 8). Moreover, we do not observe α5 subunit dynamics (Fig. 7),

603 whereas knock-down of α5 leads to decreased levels of α2 subunits (Fig. 4), and α2
604 dynamics are no longer observable when knocking-down α5 in the MBONs of the α'3
605 compartment (Fig. 7). Thus, we can draw first analogies to glutamatergic systems
606 governing plasticity in vertebrates. Whether more core criteria are met for the
607 comparison of invertebrate and vertebrate plasticity systems, further depends on
608 whether the here observed receptor dynamics will actually translate to exo-
609 /endocytosis of postsynaptic receptors or lateral diffusion of receptor subunits along
610 the MBON dendrites. Our established system should provide the means to investigate
611 this further in the future.
612
613 Interestingly, high levels of dendritic activation after α5 knock-down are
614 translated to reduced axonal calcium transients[4], effectively leading to decreased
615 signal transduction within the MBON. Of note, MBONs do not appear to exhibit
616 prominent spines on their dendrites[23] (but see section below: *Are cholinergic and*
617 *glutamatergic synapses interchangeable?*). Therefore, increased dendritic activation
618 could lead to a change in membrane resistance and result in synaptic interference.
619
620
621 ***α2 subunit-positive receptors mediate memory expression***
622
623 We also find that later forms of appetitive memory expression require both the
624 α2 and α1 receptor subunits (Fig. 2). A recent study[37] has demonstrated that, when
625 expressed heterologously, these subunits can co-assemble to form heterodimers with
626 β subunits, which, depending on the precise composition of these channels, can harbor
627 different properties, potentially reminiscent to AMPAR[55]. However, MB distribution
628 profiles of α1 and α2 subunits do not match completely, for instance at the level of the
629 γ5 or α'2 compartments (Fig. 4), indicating that they could also partake in different or
630 independent receptor configurations. It would be worthwhile to compare receptor
631 localization with single cell sequencing results[8].
632
633 Importantly, α2 subunit knock-down at M4/6 MBONs does not affect immediate
634 appetitive memories, but later stages of memory (Fig. 2). We show in a complex
635 neuropile, that *in vivo*, on a time scale of 10 to 20 minutes after learning, exposure to
636 odor induces changed α2 receptor subunit dynamics (signal recovery after
637 photobleaching) that are suppressed by simultaneous dopamine exposure ('learning',
638 Fig. 6). Therefore, changes in α2 dynamics could match the temporal profiles of

639 memory expression and consolidation processes taking place in an early phase
640 following training (the first 20 minutes) to establish longer-term memories (3 hours). It
641 should be noted that, whether dopamine pairing would also lead to a reduction of α2
642 levels over time, potentially explaining synaptic depression, cannot be assessed with
643 our experimental settings at this time, but would appear as a valid possibility.
644
645 We show that familiarity learning can take place when knocking down α2
646 nAChR subunits in α'3 MBONs in principle (Fig. 8), however, at clearly decreased
647 efficacy and only after several trials. We speculate that the observation of memories
648 still being expressed *per se* in this context, could be explained by redundancies with
649 α1 or other subunits (but see heterogeneous localization and enrichment in different
650 MB compartments, Fig. 4). Redundancies could also explain why we partially observe
651 functional phenotypes after knock-down of individual subunits, but only moderate
652 structural changes. We also would like to point out that subunits we did not identify as
653 absolutely required for memory expression (Fig. 2) in this study could nonetheless
654 partake in distinct phases of plasticity processes.
655
656 Similar to AMPAR, localization of α2, but not α5 subunits, depends on Dlg, the
657 orthologue to vertebrate PSD-95 and PSD-93. Interestingly, the latter has been
658 implicated in structural integrity of cholinergic nicotinic receptor arrangements[59] in
659 vertebrates.
660
661
662 ***α2 dynamics as general plasticity mode?***
663
664 In the context of both familiarity learning and appetitive conditioning, odor
665 exposure induces increased α2 subunit dynamics (Fig. 6, 7) accompanying
666 postsynaptic depression[7,15] (Fig. 7), while not or mildly affecting α5 subunits (for
667 familiarity learning). Therefore, the same basic mechanisms, odor-induced α2 receptor
668 dynamics, seem to express two opposed plastic outcomes in the context of associative
669 and non-associative memories and contribute to different learning rules across MB
670 compartments[22,56]. We speculate that α2 dynamics induced by odor in the M4/6
671 dendrites could be reminiscent of dark currents in the vertebrate visual system[57]
672 allowing for rapid adaptation with low levels of synaptic noise. Receptor exchange at
673 the level of M4/6 dendrites would actually take place when no associations are formed
674 and stalled when dopaminergic neurons (triggered by sugar) are simultaneously active

675 with KCs (triggered by odor). Indeed, repeated OCT stimulation led to a facilitation of
676 calcium transients (potentially corresponding to an increase of receptor incorporation,
677 Fig. 5-6), while depression (in this case likely to be mediated by removal of receptors,
678 but see above) is triggered by paired training (Fig. 5). In contrast, at the level of the α'3
679 compartments, odor activates both MBONs and dopaminergic neurons. Here, the
680 plasticity rule would be reversed. Synaptic depression is accompanied by actively
681 changing the receptor composite. We speculate that such plasticity could function
682 reminiscent of mechanisms observed for climbing fiber-induced depression of parallel
683 fiber to Purkinje cell synapses[58]. However, whether increased dynamics can be
684 translated to more incorporation or removal of α2-type receptors, or depending on the
685 plasticity rule both, will require high resolution imaging experiments in the future.
686
687
688 ***Are cholinergic and glutamatergic synapses interchangeable?***
689
690 Our study fuels the question of how unique properties of individual
691 neurotransmitter systems at synapses are. While dopamine signaling is remarkably
692 conserved between invertebrates and vertebrates, cholinergic and glutamatergic
693 systems appear, now more than before (with this study), somewhat interchangeable.
694 While vertebrates (but also evolutionarily distant *C. elegans*) for instance use
695 acetylcholine at the neuromuscular junction and store memories predominantly at
696 glutamatergic synapses, it is the other way around in *Drosophila* and other
697 invertebrates, such as *Sepia*[4–6,60,61]. Now we show that, at cholinergic synapses, α5
698 and α2 subunits, at least to a certain extent, behave in a potentially comparable way
699 to NMDARs and AMPARs at glutamatergic synapses during postsynaptic plasticity
700 which underlies memory storage. In this context, we offer several lines of evidence that
701 invertebrates utilize postsynaptic plasticity during memory storage and not as
702 previously assumed rely on presynaptic mechanisms only.
703
704 We therefore propose that, across phyla, postsynaptic plasticity, with the
705 propensity to store memories and adapt network function plastically, can take place
706 regardless of neurotransmitter identity.
707
708 One key difference between the dendritic arbors of the MBONs analyzed in this
709 study compared to dendrites of glutamatergic neurons in vertebrates, is a lack of
710 anatomical spines (Supplementary Fig. 9a). Without spines, how can input-specificity

711 be preserved at MBON postsynaptic densities? KC output to MBON input analysis of
712 the recently published fly hemibrain connectome[62] (neuprint.org) suggests that, at the
713 ultrastructural level, MBON postsynaptic densities are separated spatially
714 (Supplementary Fig. 9a). Compartmentalization could therefore be mediated by, for
715 instance, biochemical separation of PSDs. Importantly, input-specific plasticity has
716 been shown to be inducible in non-spiny neurons in vertebrates, with diffusion barriers
717 established, e.g., through calcium buffers, between postsynaptic densities[63].
718
719 Interestingly, our MBON input analysis further revealed that postsynaptic
720 plasticity mechanisms could actually add a layer to promote input-specificity. Indeed,
721 we find that single presynaptic KC release sites that innervate MBON dendrites can
722 also target other MBONs and/or other postsynaptic targets simultaneously
723 (Supplementary Fig. 9b-f). Plasticity confined to single postsynaptic densities
724 innervated by a KC terminal could therefore change the weight of transmission for one
725 target (e.g., MBONs involved in memory storage, such as M4[7]), while not changing the
726 weight of the connection to other targets (for example MBONs not involved in a specific
727 action or other targets of non-MBON identity, Supplementary Fig. 9g). It should be
728 noted that this architecture does not exclude presynaptic plasticity mechanisms[70] (for
729 instance following aversive conditioning). Indeed, we would speculate that synaptic
730 connections can be subdivided into distinct compartments on both the pre- and the
731 postsynaptic side, potentially through transsynaptic molecules[61,64], allowing for fine-
732 tuned and target-dependent changes of parameters within either side of a synapse.
733
734
735 ***A molecular plasticity sequence?***
736
737 Together, we propose a model (Fig. 9) in which α5-subunit containing receptors
738 could mediate the early phase of postsynaptic memory storage and we speculate this
739 could lead to elevated postsynaptic calcium flux (not addressed in this study).
740 Concurrent events see changed dynamics of the α2 receptor. Nicotinic receptor
741 subunits hereby could interact with adaptor proteins to bind to Dlg, reminiscent to what
742 is known for AMPAR[35]. Importantly, we identify elevated α2 subunit dynamics in the
743 context of associative and non-associative memory expression. Increased α2 subunit
744 dynamics in both cases are triggered by odor application. At the level of M4/6,
745 suppressed dynamics would correspond to synaptic depression, while at the level of
746 α'3 MBONs increased dynamics may result in postsynaptic depression. Therefore,

747 different learning rules could govern the incorporation or exchange or mobilization of
748 receptors in or out of synapses. The precise molecular and biophysical parameters
749 underlying these plasticity rules are currently unknown and will need to be addressed
750 in the future. One option could include potential exchange of α2 subunits for a receptor
751 complex with higher calcium permeability.
752
753 Our findings are consistent with the current mushroom body skew model[5],
754 where the summed MBON output will determine an animal's choice. However, we add
755 an additional layer, already at the MBON input site. Changes do not happen, as
756 previously believed, at the presynaptic compartment only, but potentially at both
757 synaptic compartments. Thus, the power to store (potentially conflicting) information
758 separately at either the pre- or postsynaptic site, equips the system with additional
759 flexibility. How precisely pre- to postsynaptic and post- to presynaptic signaling is
760 regulated will need to be addressed in the future, but will likely involve transsynaptic
761 signaling routes[61,64]. Importantly, the identified modes of postsynaptic plasticity will
762 open avenues for investigations looking into pre- versus postsynaptic contributions
763 during reversal learning, reconsolidation and extinction learning[13,33].
764
765

766 **Methods**

767 ***Fly genetics***

768 Flies were raised on standard food under standard laboratory conditions unless
769 stated otherwise (25°C, 65 %, 12-hour light-dark cycle)[7,40]. Driver lines used were
770 MB011B (Split-Gal4)[10], MB112C[10] (Split-Gal4), MB461B[10] (Split-Gal4), MB027B[15]
771 (Split-Gal4), R13F02-Gal4[10], OK107-Gal4[4], VT1211-GAL4[7], and R58E02-LexA[26]. We
772 used the following UAS-nAChR^{RNAi} flies[4,51]: Bloomington stock numbers 28688, 27493,
773 27671, 31985, 25943, 27251 and 25835. Additionally, we used[41,42] Dlg^{S97}-RNAi as well
774 as UAS-Dlg^{GFP}, tubP-GAL80^{ts} [48], UAS-Shi^{ts1} [48], 247-dsRed[7], LexAop-CsChrimson,
775 UAS-GCamp6f[4,13,26], and UAS-SynaptoPhluorin[65]. Gal80^{ts} flies were raised at 18-20°C
776 and were placed at 32°C 3-5 days before the experiment. Note that complex genotypes
777 did not always permit usage of MB011B for genetical access to M4/6 neurons
778 throughout the manuscript. In that case, in order to reduce genetic complexity, we used
779 VT1211-Gal4.

780 ## *Behavior*

781 ### *T-maze memory*

782 3-9-day old mixed-sex populations were trained and tested together as
783 previously described[7]. Odors used were 3-Octanol (OCT, Aldrich) and 4-
784 Methylcyclohexanol (MCH, Aldrich) diluted in mineral oil (approximately 1:100 for
785 aversive, 1:1000 for appetitive memory, absolute concentrations were minimally
786 adjusted to prevent odor bias). For aversive protocols, flies were exposed to the CS+
787 for 1 minute with 12 1.5 seconds long 120 V electric shocks (interstimulus interval: 3.5
788 seconds) followed by 45 seconds of air, 1 minute of CS- exposure and another 30
789 seconds of air. Flies were given 2 minutes to choose between the CS+ and CS- in a
790 T-Maze during retrieval in the dark. For appetitive conditioning flies were starved for
791 20 - 24 hours before the experiment. Flies were exposed to the CS- for 2 minutes. After
792 30 seconds, flies were exposed to the CS+ paired with sugar for 2 minutes followed by
793 another 30 seconds of air. Performance indices were calculated as described
794 previously[7]. Time of retrieval is stated in the figures. For Shi^{ts} experiments, flies were
795 kept at 32°C 30 minutes prior to and during training and brought to room temperature
796 directly afterwards. Room temperature was approximately 23°C. For Fig. 2 and
797 Supplementary Fig. 2 behavioral data sets from separate experiments were pooled.
798 Note that 'screening hit' data displayed in Fig. 2a,b and Supplementary Fig. 2a,b were
799 replotted to allow for comparison of genotypes with the corresponding genetic controls
800 in Supplementary Fig. 2i-m.

801 ### *Familiarity learning*

802 Familiarity training was essentially performed as described before[15] with slight
803 adjustments. Flies were covered in yellow dust (Reactive Yellow 86, Fisher Scientific)[15]
804 and placed in a cylindrical custom designed chamber. To ensure a constant air stream
805 we placed the chamber between an air and a vacuum pump (800ml/min). Air
806 permeable cotton wool was used to close the open ends of the chamber. The air supply
807 was either connected to pure mineral oil or MCH diluted in mineral oil at a concentration
808 of 1:50. For switching between odor and mineral oil, a clamp was manually opened
809 and closed. Video recording was performed at 26 frames per second. For recordings
810 and analyses we used Python (v3.6) in Anaconda Jupyter Notebook environment.

811

Imaging

Confocal single photon imaging and receptor quantification

Fixed explant brain imaging. Brains were dissected on ice, fixed in 4% paraformaldehyde (Sigma) for 20 minutes and placed in PBST (0.1% Triton) for 30 minutes followed by washing with PBS for 20 minutes twice. Vectashield was used as mounting medium. Flies were 2-8 day-old females raised at room temperature.

Recording endogenous fluorescence. Imaging was performed using a confocal single photon inverse microscope (Leica SP5/STED) equipped with a 64x oil objective. Laser power and gain were adjusted between experiments, making normalization of the signals necessary. Values for the heatmap in Fig. 4 were normalized to the mean MB fluorescence value to ensure comparability. Voxel size was (height x width x depth) 123 nm x 123 nm x 500 nm. ROIs were drawn manually in ImageJ using the 247-dsRed channel for orientation (Fig. 4a). Heat maps were created in Microsoft Excel. For quantifications following knock-down, the γ5 compartment was normalized to γ4 ((γ5- γ4)/ γ4), and the β'2 to the β'1 compartment ((β'2- β'1)/ β'2) of the same animal. Each 'n' corresponds to one hemisphere.

In vivo two photon imaging of receptor dynamics

Fluorescence recovery after photobleaching (FRAP) experiments were performed *in vivo*. 2-8 day-old flies were anesthetized on ice and mounted in a custom-made chamber. The head capsule was opened under room temperature sugar-free HL3-like saline, and legs were immobilized with wax[7]. Sugar-free HL3-like saline containing 30 units of Papain (Roche) was applied to the head capsule for 8 minutes to digest the brain's glial sheath and facilitate removal. Images were acquired using a multi photon microscope (Nikon) with a 25× water-immersion objective, controlled by Nikon NIS Elements software. Diluted odors (MCH or OCT in mineral oil 1:1000) were delivered on a clean air carrier stream using a 6-channel delivery system (CON electronics). The flies were subjected to experimental conditions including either no odor (air), odor only, odor paired with local dopamine (10 mM) injection via a micropipette, or local dopamine injection only (see Fig. 6b and Supplementary Fig. 6b for experimental protocol schematics). Photobleaching was accomplished using focused, high intensity laser exposure for ~1 minute. Analysis of fluorescence recovery was performed using FIJI. ROIs were manually selected and the percent recovery fluorescence was calculated by subtraction of the post-bleaching baseline

845 fluorescence and division by the pre-bleaching baseline fluorescence. The percent
846 recovery values were log-transformed and a linear mixed effects model without
847 intercept was fit using the interaction between condition and time as fixed effect - to
848 determine condition-specific differences of the recovery kinetics - and time as random
849 effect (R package lme4). A linear mixed effect model was used to appropriately model
850 repeated measures within animals. Significance of recovery of individual conditions
851 was assessed using the regression coefficients of the condition-time interaction of the
852 linear mixed model. Differences of recovery between pairs of conditions were tested
853 using pairwise comparisons of estimated marginal means of the linear mixed model (R
854 package emmeans). Correction for multiple pairwise comparisons was performed
855 using Tukey's method.

856 **In vivo *confocal single photon imaging of receptor dynamics and calcium***
857 ***transients***

858 3-4 days after eclosure, female flies were prepared as described above and
859 imaged. Imaging was performed using a SP5 single-photon confocal microscope
860 (Leica microsystems). Recording frame rate was 3 Hz. For bleaching high laser power
861 was used focusing on the α'3 compartments for 15-25 seconds. The baseline was
862 recorded after bleaching, immediately before fixed inter-stimulus interval-training[15].
863 OCT was presented ten times for a second with a six second pause in between. Odor
864 delivery (CON electronics) was controlled by the Leica acquisition software. After
865 training, the same brain plane was recorded for 10 seconds with a pixel size of 200 nm
866 in time intervals of 0, 5, 10, 15, 20, 30, 60 minutes after training. For control
867 experiments air only was delivered to the chamber. Images of the same time interval
868 recordings were averaged and processed in ImageJ. Gaussian blur (σ = 0.5) was
869 applied for smoothing and ROIs were selected manually.

870 **In vivo *two photon calcium imaging***

871 To measure odor responses, female 3-6-day old flies expressing UAS-
872 GCaMP6f and UAS-RNAi to α2 or α5 at the level of M4/6 were tethered under the
873 multiphoton microscope (Femtonics), essentially as described before[7,66]. 5 alternating
874 1 second OCT and MCH puffs were applied with 30 seconds in between each
875 presentation. Fluorescent signals were recorded from dendrites in the β'2 MB
876 compartment using MESc software (Femtonics) at a frame rate of roughly 31 Hz. ROIs
877 incorporating the dendritic arbors were manually drawn. Data was processed using a
878 Savitzky-Golay filter. Further analysis was performed using Matlab. For absolute

879 training, following protocol was applied: after initial testing for odor responses, flies
880 were exposed to odor puffs (MCH) twice with a 30-second gap between the
881 applications. Corresponding odor responses were averaged. Training consisted of
882 odor application while the fly fed on a sucrose droplet provided by a custom-made
883 feeding arm[67]. After a two-minute break, two odor puffs with a gap of 30 seconds were
884 applied. Again, corresponding odor responses were averaged. Areas under the curve
885 (AUCs) were calculated using Matlab and the first 4 seconds following odor onset were
886 analyzed in order to cover entire responses. The AUCs pre- and post-training were
887 normalized to the mean pre-training values of a group respectively. The averaged test
888 responses pre-training were compared to the average post-training responses using a
889 paired t-test or Wilcoxon matched-pairs signed rank test.

890 ***Explant brain widefield imaging, neurotransmitter application and optogenetics***

891 *Postsynaptic plasticity induction:* Brains of 3-10 day-old mixed sex flies were
892 dissected on ice. Flies expressed CsChrimson^{tdTomato} under control of R58E02-LexA
893 and UAS-GCaMP6f (and α2 RNAi) under control of MB011B. The head capsule and
894 sheath were removed in carbogenated solution (103 mM NaCl, 3 mM KCl, 5 mM N-
895 Tris, 10 mM trehalose, 10 mM glucose, 7 mM sucrose, 26 mM $NaHCO_3$, 1 mM
896 NaH_2PO4, 1.5 mM $CaCl_2$, 4 mM $MgCl_2$, 295 mOsm, pH 7.3) with forceps. The brain
897 was subsequently perfused with carbogenated solution containing TTX (2 µM; 20 ml /
898 10 min flow speed) and imaged using an Olympus MX51WI wide field microscope with
899 a 40x Olympus LUMPLFLN objective and an Andor iXON Ultra camera controlled by
900 Solis software. An Olympus U25ND25 light filter was placed in the beam path to
901 minimize baseline CsChrimson activation. A custom designed glass microcapillary was
902 loaded with uncarbongenated solution containing 0.1 mM acetylcholine and
903 maneuvered to the M6 dendrites. The injection pressure of a P25-1-900 picospritzer
904 was calibrated between 3-8 psi (depending on initial calcium responses). Each local
905 acetylcholine application spanned 15 ms with a 4 s inter-injection interval.

906 Three pulses of acetylcholine followed by a 2-3 minute break were recorded
907 after which the optogenetic response was assessed by applying 2 seconds red light
908 pulses with an inter-red light-interval of 4 seconds. 3 acetylcholine pulses were
909 recorded followed by either 5 acetylcholine injections, 5 red light pulses or both paired.
910 For paired training both stimuli began simultaneously and the acetylcholine injection
911 lasted for 15 ms (and gave rise to a calcium transients typically lasting > 1 seconds,
912 please see example in Fig. 3), while the paired red light pulse lasts for 2 seconds,
913 allowing for maximal temporal overlap. This process was repeated 5x, with a 4 second

914 break between trials. Following the training trial, 3 final acetylcholine test injections
915 were applied after 1 minute. For analysis, the first of the 3 acetylcholine injections was
916 always discarded because of initial dilution of the capillary tip and the remaining 2 peak
917 intensities were averaged.

918 All peaks within an experiment were quantified relative to the fluorescence
919 baseline that we calculated for pre and post training acetylcholine responses.
920 Baselines were set independently for each pre- and post-training recording using the
921 polynomial interpolation function in NOSA[68]. For investigating α2 knock-down, only the
922 paired condition was tested.

923 For controls not expressing CsChrimson, we used VT1211-Gal4 driving UAS-
924 GCaMP6f, instead of MB011B, for technical reasons. This was combined with either
925 expression of R58E02-LexA or LexAop-CsChrimson^{tdTomato}. Only paired training was
926 investigated in this context.

927 *Excitability of Kenyon cell axons:* To test whether KC axons were excited by
928 focal acetylcholine injections at the level of M4/6 dendrite innervation, either UAS-
929 SynaptoPhluorin or UAS-GCaMP6f were expressed under the control of OK107-Gal4.
930 Following the acetylcholine injection experiment, the capillary was exchanged with a
931 capillary containing the same solution with additional 300-400 mM KCl, to evaluate
932 tissue health (not shown for GCaMP6f imaging). To pick up potentially small changes,
933 we increased the injection pressure to 8-14 Psi and the injection time to 150-225 ms
934 (GCaMP6f, 8s inter-injection interval and 3 consecutive injections) and 300-525 ms
935 (SynaptoPhluorin, with an 8s inter-injection interval and 3 consecutive injections).

936 Images were analyzed using NOSA[40,68] and GraphPad Prism.

937

938 ## Statistics

939 Statistical analyses were performed as stated in the previous methods sections
940 and figure legends. Data were always tested for normality using a Shapiro-Wilk test. If
941 normally distributed, data were analyzed using ANOVA followed by post-hoc test or a
942 (paired) t-test. If not normal, we used a Kruskal Wallis followed by post-hoc test, or a
943 Wilcoxon matched-pairs signed rank test.

944

Tagged receptor subunits

All subunits were tagged using CRISPR technology and motifs previously described[69]. Further details will be published separately and can be requested from the corresponding author.

Connectome analysis

In Supplementary Fig. 9, we analyzed the partial connectome of the female adult fly brain (hemibrain v1.2.1)[62] using the neuprint-python package (https://github.com/connectome-neuprint/neuprintpython). To investigate the synaptic relationship between KC presynapses and MBON postsynaptic sites, we first identified KCs with the status 'Traced' in the connectome. Second, for each MBON of interest, we identified the relevant KCs connected to it (which is a subset of the count in the previous step). Third, for each KC identified, we selected each presynaptic terminal (x,y,z locations of synapses) connected to the MBON of interest, and for each of these presynapses, we identified all synaptic partners residing on the postsynaptic side. Fourth, for the MBON of interest, we counted the number of postsynaptic connections per individual presynapses (that also contain the specific MBON, Supplementary Fig. 9 d,e,f). Finally, we identified the composition of all neurons identified as co-postsynaptic partners of KC to MBON synapses.

Data availability

The datasets generated during and/or analysed during the current study are available from the corresponding author on reasonable request.

Code availability

The code used in this study is available at
https://github.com/jagannathancolabs/2022_postsynapticplasticity

Acknowledgements

We thank Anatoli Ender, Johannes Felsenberg, Davide Raccuglia, Lisa Scheunemann, Stephan Sigrist, Uli Thomas and Scott Waddell for comments on the manuscript, Stephan Sigrist and Uli Thomas for reagents, the Janelia and Vienna fly projects, and the Bloomington Stock Center and VDRC for fly lines as well as Daisuke Hattori and Yoshi Aso for help with the familiarity experiments. Multiphoton and single photon confocal imaging was partially performed using microscopes of the AMBIO and NWFZ core facilities of the Charité. **Funding:** Funded by the Deutsche Forschungsgemeinschaft (DFG, German Research Foundation) under Germany´s Excellence Strategy – EXC-2049 – 390688087, the Emmy Noether Programme, TP A27 of SFB958 (184695641), and TP A07 of SFB1315 (327654276) to DO. S.R.J is supported by the Walter Benjamin Programme of the DFG. **Author contribution**: Conceptualization, C.P., M-M.H., E.R., S.R., D.L., Y-C.C., D.O., Investigation, C.P., M-M.H., E.R. D.L., R.S.-G., C.R., S.R., Y-C.C., I.B., T.F., G.L., S.R.J.; Resources, D.O.; Writing, D.O., C.P.; Instrumentation: JR; Comments, M-M.H., E.R. D.L., R.S.-G., S.R., Y-C.C., S.R.J..

Competing interests: Authors declare no competing interests.

Supplemental Information:

Supplementary Figure 1. Permissive temperature controls accompanying Fig. 1.

Supplementary Figure 2. Genetic controls and alternate data display accompanying Fig. 2.

Supplementary Figure 3. Control experiments for Fig. 3.

Supplementary Figure 4. Detailed distribution of α subunits in the MB accompanying Fig. 4.

Supplementary Figure 5. Additional data accompanying Fig. 5.

Supplementary Fig. 6. Receptor subunit recovery, accompanying Fig. 6.

1011

1012 Supplementary Fig. 7. Dlg^{GFP} FRAP, accompanying Fig. 7.

1013

1014 Supplementary Fig. 8. Additional ethograms, accompanying Fig. 8.

1015

1016 Supplementary Fig. 9. Input analysis of KC to MBON synapses, referred to in legend
1017 of Fig. 9.

1018

1019 References

1020 1. Glanzman, D. L. Common Mechanisms of Synaptic Plasticity in Vertebrates and
1021 Invertebrates. Curr Biol 20, R31–R36 (2010).
1022
1023 2. Korte, M. & Schmitz, D. Cellular and System Biology of Memory: Timing, Molecules,
1024 and Beyond. Physiol Rev 96, 647–93 (2016).
1025
1026 3. Nicoll, R. A. A Brief History of Long-Term Potentiation. Neuron 93, 281–290 (2017).
1027
1028 4. Barnstedt, O. et al. Memory-Relevant Mushroom Body Output Synapses Are
1029 Cholinergic. Neuron 89, 1237–47 (2016).
1030
1031 5. Owald, D. & Waddell, S. Olfactory learning skews mushroom body output pathways
1032 to steer behavioral choice in Drosophila. Curr Opin Neurobiol 35, 178–84 (2015).
1033
1034 6. Shomrat, T. et al. Alternative sites of synaptic plasticity in two homologous “fan-out
1035 fan-in” learning and memory networks. Curr Biology Cb 21, 1773–82 (2011).
1036
1037 7. Owald, D. et al. Activity of Defined Mushroom Body Output Neurons Underlies
1038 Learned Olfactory Behavior in Drosophila. Neuron 86, 417–427 (2015).
1039
1040 8. Aso, Y. et al. Nitric oxide acts as a cotransmitter in a subset of dopaminergic neurons
1041 to diversify memory dynamics. Elife 8, e49257 (2019).
1042
1043 9. Aso, Y. et al. Mushroom body output neurons encode valence and guide memory-
1044 based action selection in Drosophila. Elife 3, e04580 (2014).
1045
1046 10. Aso, Y. et al. The neuronal architecture of the mushroom body provides a logic for
1047 associative learning. Elife 3, e04577 (2014).
1048
1049 11. Bouzaiane, E., Trannoy, S., Scheunemann, L., Plaçais, P.-Y. & Preat, T. Two
1050 independent mushroom body output circuits retrieve the six discrete components of
1051 Drosophila aversive memory. Cell Reports 11, 1280–92 (2015).
1052
1053 12. Cohn, R., Morantte, I. & Ruta, V. Coordinated and Compartmentalized
1054 Neuromodulation Shapes Sensory Processing in Drosophila. Cell 163, 1742–55
1055 (2015).
1056
1057 13. Felsenberg, J. et al. Integration of Parallel Opposing Memories Underlies Memory
1058 Extinction. Cell 175, 709-722.e15 (2018).
1059

14. Felsenberg, J., Barnstedt, O., Cognigni, P., Lin, S. & Waddell, S. Re-evaluation of learned information in Drosophila. Nature 544, 240–244 (2017).

15. Hattori, D. et al. Representations of Novelty and Familiarity in a Mushroom Body Compartment. Cell 169, 956-969.e17 (2017).

16. Ichinose, T. et al. Reward signal in a recurrent circuit drives appetitive long-term memory formation. Elife 4, e10719 (2015).

17. Lewis, L. P. C. et al. A Higher Brain Circuit for Immediate Integration of Conflicting Sensory Information in Drosophila. Curr Biology Cb 25, 2203–14 (2015).

18. Pai, T.-P. et al. Drosophila ORB protein in two mushroom body output neurons is necessary for long-term memory formation. P Natl Acad Sci Usa 110, 7898–903 (2013).

19. Perisse, E. et al. Aversive Learning and Appetitive Motivation Toggle Feed-Forward Inhibition in the Drosophila Mushroom Body. Neuron 90, 1086–99 (2016).

20. Séjourné, J. et al. Mushroom body efferent neurons responsible for aversive olfactory memory retrieval in Drosophila. Nat Neurosci 14, 903–10 (2011).

21. Plaçais, P.-Y., Trannoy, S., Friedrich, A. B., Tanimoto, H. & Preat, T. Two pairs of mushroom body efferent neurons are required for appetitive long-term memory retrieval in Drosophila. Cell Reports 5, 769–80 (2013).

22. Hige, T., Aso, Y., Modi, M. N., Rubin, G. M. & Turner, G. C. Heterosynaptic Plasticity Underlies Aversive Olfactory Learning in Drosophila. Neuron 88, 985–98 (2015).

23. Takemura, S. et al. A connectome of a learning and memory center in the adult Drosophila brain. Elife 6, e26975 (2017).

24. Bilz, F., Geurten, B. R. H., Hancock, C. E., Widmann, A. & Fiala, A. Visualization of a Distributed Synaptic Memory Code in the Drosophila Brain. Neuron 106, 963-976.e4 (2020).

25. Boto, T., Louis, T., Jindachomthong, K., Jalink, K. & Tomchik, S. M. Dopaminergic modulation of cAMP drives nonlinear plasticity across the Drosophila mushroom body lobes. Curr Biology Cb 24, 822–31 (2014).

26. Handler, A. et al. Distinct Dopamine Receptor Pathways Underlie the Temporal Sensitivity of Associative Learning. Cell 178, 60-75.e19 (2019).

27. Ehmann, N., Owald, D. & Kittel, R. J. Drosophila active zones: from molecules to behaviour. Neurosci Res 127, 14–24 (2017).

28. Dubnau, J., Grady, L., Kitamoto, T. & Tully, T. Disruption of neurotransmission in Drosophila mushroom body blocks retrieval but not acquisition of memory. Nature 411, 476–480 (2001).

29. Krashes, M. J., Keene, A. C., Leung, B., Armstrong, J. D. & Waddell, S. Sequential Use of Mushroom Body Neuron Subsets during Drosophila Odor Memory Processing. Neuron 53, 103–115 (2007).

30. McGuire, S. E., Le, P. T. & Davis, R. L. The Role of Drosophila Mushroom Body Signaling in Olfactory Memory. Science 293, 1330–1333 (2001).

31. Schwaerzel, M., Heisenberg, M. & Zars, T. Extinction Antagonizes Olfactory Memory at the Subcellular Level. Neuron 35, 951–960 (2002).

32. Kandel, E. R., Dudai, Y. & Mayford, M. R. The molecular and systems biology of memory. Cell 157, 163–86 (2014).

33. Lüscher, C. & Malenka, R. C. Drug-evoked synaptic plasticity in addiction: from molecular changes to circuit remodeling. Neuron 69, 650–63 (2011).

34. Won, S., Levy, J. M., Nicoll, R. A. & Roche, K. W. MAGUKs: multifaceted synaptic organizers. Curr Opin Neurobiol 43, 94–101 (2017).

35. Thompson, A. J., Lester, H. A. & Lummis, S. C. R. The structural basis of function in Cys-loop receptors. Q Rev Biophys 43, 449–99 (2010).

36. Dent, J. A. Advances in Experimental Medicine and Biology. Adv Exp Med Biol 683, 11–23 (2010).

37. Ihara, M. et al. Cofactor-enabled functional expression of fruit fly, honeybee, and bumblebee nicotinic receptors reveals picomolar neonicotinoid actions. Proc National Acad Sci 117, 16283–16291 (2020).

38. Lansdell, S. J., Collins, T., Goodchild, J. & Millar, N. S. The Drosophila nicotinic acetylcholine receptor subunits Dα5 and Dα7 form functional homomeric and heteromeric ion channels. Bmc Neurosci 13, 73 (2012).

39. Eadaim, A., Hahm, E.-T., Justice, E. D. & Tsunoda, S. Cholinergic Synaptic Homeostasis Is Tuned by an NFAT-Mediated α7 nAChR-Kv4/Shal Coupled Regulatory System. Cell Reports 32, 108119 (2020).

40. Raccuglia, D. et al. Network-Specific Synchronization of Electrical Slow-Wave Oscillations Regulates Sleep Drive in Drosophila. Curr Biology Cb 29, 3611-3621.e3 (2019).

41. Bachmann, A. et al. Cell type-specific recruitment of Drosophila Lin-7 to distinct MAGUK-based protein complexes defines novel roles for Sdt and Dlg-S97. J Cell Sci 117, 1899–1909 (2004).

42. Soukup, S.-F., Pocha, S. M., Yuan, M. & Knust, E. DLin-7 Is Required in Postsynaptic Lamina Neurons to Prevent Light-Induced Photoreceptor Degeneration in Drosophila. Curr Biol 23, 1349–1354 (2013).

43. Crittenden, J. R., Skoulakis, E. M., Han, K. A., Kalderon, D. & Davis, R. L. Tripartite mushroom body architecture revealed by antigenic markers. Learn Mem Cold Spring Harb N Y 5, 38–51 (1998).

44. Eichler, K. et al. The complete connectome of a learning and memory centre in an insect brain. Nature 548, 175–182 (2017).

45. Stuart, G. J. & Spruston, N. Dendritic integration: 60 years of progress. Nat Neurosci 18, 1713–1721 (2015).

46. Tully, T., Preat, T., Boynton, S. C. & Vecchio, M. D. Genetic dissection of consolidated memory in Drosophila. Cell 79, 35–47 (1994).

47. Trannoy, S., Redt-Clouet, C., Dura, J.-M. & Preat, T. Parallel Processing of Appetitive Short- and Long-Term Memories In Drosophila. Curr Biol 21, 1647–1653 (2011).

48. Perisse, E. et al. Different kenyon cell populations drive learned approach and avoidance in Drosophila. Neuron 79, 945–56 (2013).

49. Honegger, K. S., Campbell, R. A. A. & Turner, G. C. Cellular-resolution population imaging reveals robust sparse coding in the Drosophila mushroom body. J Neurosci Official J Soc Neurosci 31, 11772–85 (2011).

50. Zhao, X., Lenek, D., Dag, U., Dickson, B. & Keleman, K. Persistent activity in a recurrent circuit underlies courtship memory in Drosophila. Elife 7, e31425 (2018).

51. Cervantes-Sandoval, I., Phan, A., Chakraborty, M. & Davis, R. L. Reciprocal synapses between mushroom body and dopamine neurons form a positive feedback loop required for learning. Elife 6, e23789 (2017).

52. Ueno, K. et al. Carbon Monoxide, a Retrograde Messenger Generated in Postsynaptic Mushroom Body Neurons, Evokes Noncanonical Dopamine Release. J Neurosci Official J Soc Neurosci 40, 3533–3548 (2020).

53. Ueno, K. et al. Coincident postsynaptic activity gates presynaptic dopamine release to induce plasticity in Drosophila mushroom bodies. Elife 6, e21076 (2017).

54. Bliss, T. V. & Lomo, T. Long-lasting potentiation of synaptic transmission in the dentate area of the anaesthetized rabbit following stimulation of the perforant path. J Physiology 232, 331–56 (1973).

55. Greger, I. H., Watson, J. F. & Cull-Candy, S. G. Structural and Functional Architecture of AMPA-Type Glutamate Receptors and Their Auxiliary Proteins. Neuron 94, 713–730 (2017).

56. Aso, Y. & Rubin, G. M. Dopaminergic neurons write and update memories with cell-type-specific rules. Elife 5, e16135 (2016).

57. Hagins, W. A., Penn, R. D. & Yoshikami, S. Dark Current and Photocurrent in Retinal Rods. Biophys J 10, 380–412 (1970).

58. Ito, M. Cerebellar Long-Term Depression: Characterization, Signal Transduction, and Functional Roles. Physiol Rev 81, 1143–1195 (2001).

59. Neff, R. A., Gomez-Varela, D., Fernandes, C. C. & Berg, D. K. Postsynaptic scaffolds for nicotinic receptors on neurons. Acta Pharmacol Sin 30, 694–701 (2009).

60. Ackermann, F., Waites, C. L. & Garner, C. C. Presynaptic active zones in invertebrates and vertebrates. Embo Rep 16, 923–38 (2015).

61. Owald, D. & Sigrist, S. J. Assembling the presynaptic active zone. Curr Opin Neurobiol 19, 311–8 (2009).

62. Scheffer, L. K. et al. A connectome and analysis of the adult Drosophila centralbrain. Elife 9, e57443 (2020).

63. Goldberg, H., Tamas, G., Aronov, D. & Yuste, R. Calcium Microdomains in Aspiny Dendrites. Neuron 40, 807-821 (2003).

64. Tang, A.-H. et al. A transsynaptic nanocolumn aligns neurotransmitter release to receptors. Nature 536, 210-214 (2016).

65. Lin, A. C., Bygrave, A. M., Calignon, A. de, Lee, T. & Miesenböck, G. Sparse, decorrelated odor coding in the mushroom body enhances learned odor discrimination. Nat Neurosci 17, 559–568 (2014).

66. Böhme, M. A. et al. Rapid active zone remodeling consolidates presynaptic potentiation. Nat Commun 10, 1085 (2019).

67. Lin, S. et al. Neural correlates of water reward in thirsty Drosophila. Nat Neurosci 17, 1536–1542 (2014).

68. Oltmanns, S. et al. NOSA, an Analytical Toolbox for Multicellular Optical Electrophysiology. Front Neurosci-switz 14, 712 (2020).

69. Raghu, S. V., Joesch, M., Sigrist, S. J., Borst, A. & Reiff, D. F. Synaptic Organization of Lobula Plate Tangential Cells in Drosophila: Dα7 Cholinergic Receptors. J Neurogenet 23, 200–209 (2009).

70. Stahl, A. *et al.* Associative learning drives longitudinally graded presynaptic plasticity of neurotransmitter release along axonal compartments. *Elife* **11**, e76712 (2022).

Figures

Figure 1

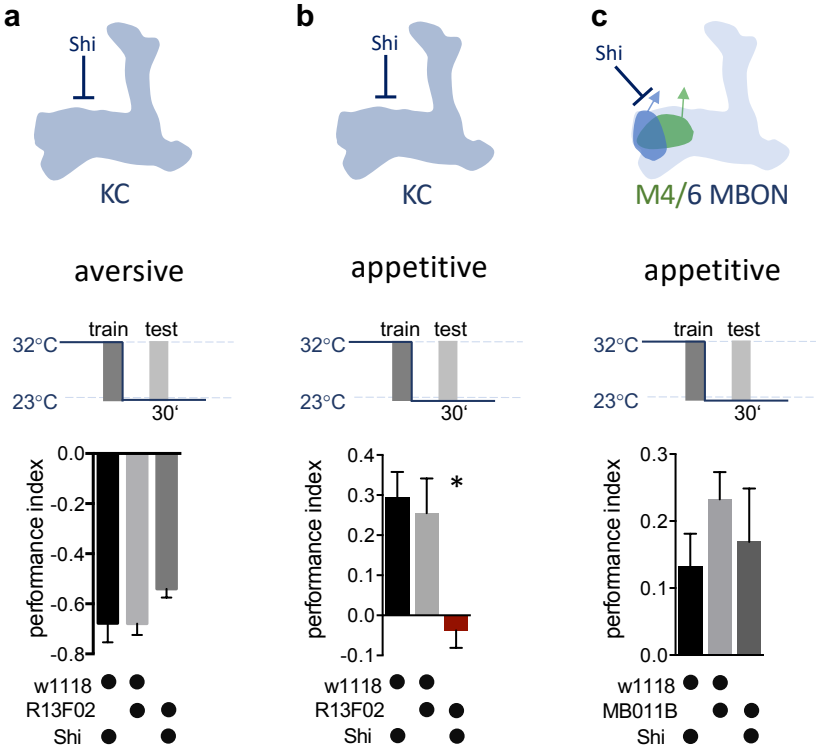

Figure 1: KC neurotransmitter release is required for the acquisition of appetitive memories.

a-c) Flies expressing temperature-sensitive Shibire (Shi) within KCs or MBONs are trained at restrictive temperature (32°C), and subsequently placed at permissive temperature (23°C) throughout the consolidation and retrieval phase. Memory performance was tested 30 minutes after training at permissive temperature. Shi blocks neurotransmitter release at 32°C.

a) Block of neurotransmitter release from KCs (driver line R13F02-Gal4) during training does not impact 30 min aversive memory performance. Bar graphs: mean ± SEM; n = 7 – 8; one-way ANOVA followed by Tukey's test ($p > 0.05$).

b) Block of neurotransmitter release from KCs (driver line R13F02-Gal4) during training impairs 30 min appetitive memory performance. Bar graphs: mean ± SEM; n = 10 – 16; Kruskal-Wallis followed by Dunn's test ($p < 0.05$), * = $p < 0.05$.

c) Block of neurotransmitter release from M4/6 MBONs (driver line MB011B) during training does not impact 30 min appetitive memory performance. Bar graphs: mean ± SEM; n = 14 – 24; one-way ANOVA followed by Tuckey's test ($p > 0.05$).

Also see Supplementary Fig. 1 for further information.

1279 **Figure 2**

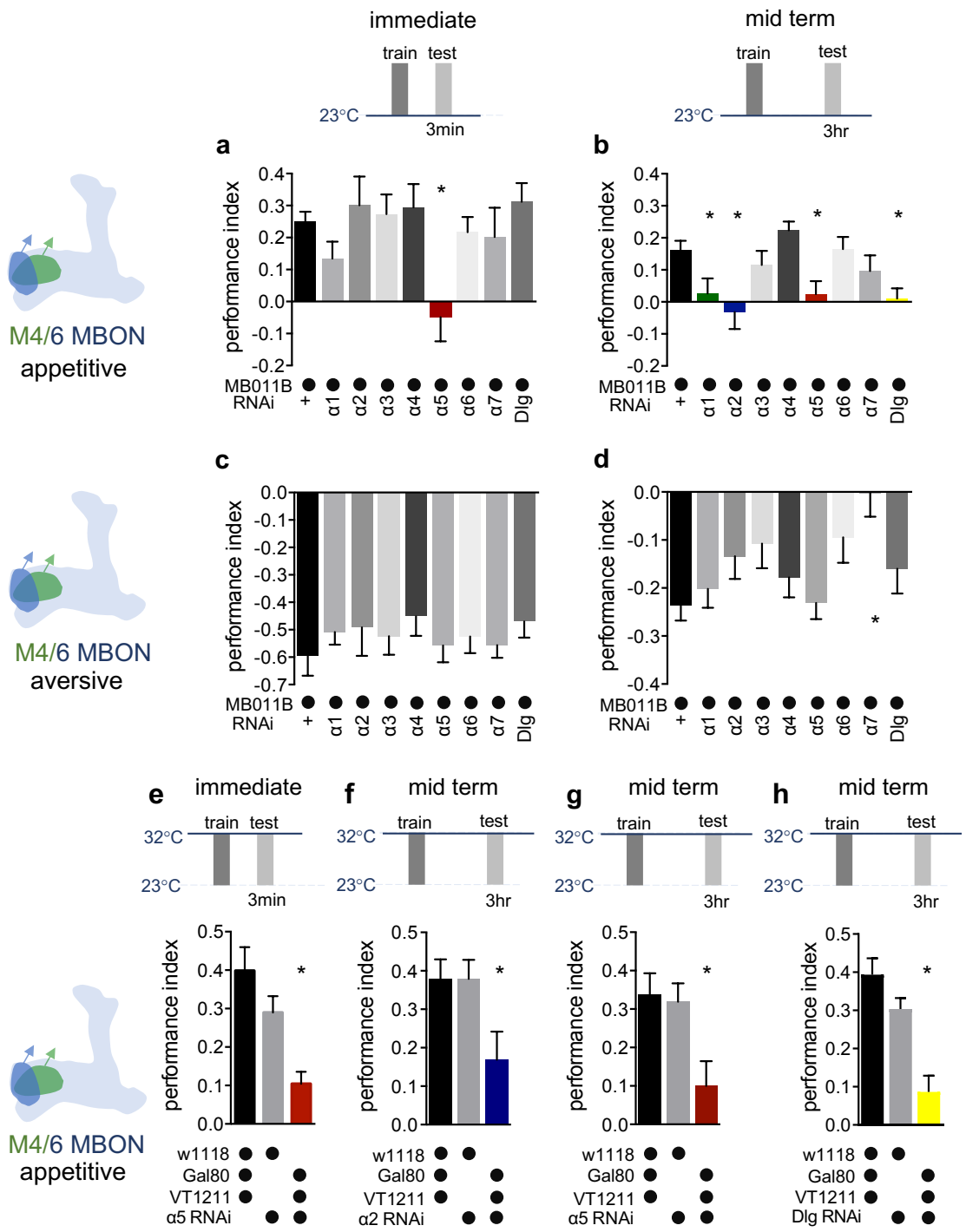

1280

1281

1282 **Figure 2: Specific nAChR α subunits are needed for specific memories in M4/6 neurons.**

1283 **a)** Immediate appetitive memories are impaired following RNAi knock-down of the α5
1284 nAChR subunit in M4/6 MBONs (driver line MB011B). Bar graphs: mean ± SEM; n = 8 – 13, for
1285 controls: n = 20; one-way ANOVA followed by Dunnett's test ($p < 0.05$), * = $p < 0.05$.

1286 Note: data depicted correspond to initial screen, please see Supplementary Fig. 2i for alternate
1287 display including all genetic controls.

1288 **b)** RNAi knock-down of the α1, α2, α5 nAChR subunits or Dlg in M4/6 MBONs (driver line
1289 MB011B) impair 3-hour appetitive memories. Bar graphs: mean ± SEM; n = 12 – 26, for
1290 controls: n = 38; Kruskal-Wallis followed by Dunn's test ($p < 0.05$), * = $p < 0.05$.

1291 Note: data depicted correspond to initial screen, please see Supplementary Fig. 2j-m for
1292 alternate display including all genetic controls.

1293 **c)** Immediate aversive learning is not impaired by RNAi knock-down of any subunit in
1294 M4/6 MBONs (driver line MB011B). Bar graphs: mean ± SEM; n = 6 – 8, for controls: n = 12;
1295 Kruskal-Wallis followed by Dunn's test ($p > 0.05$).

1296 **d)** 3-hour aversive memory is not affected by knock-down of α subunits with the exception
1297 of α7 (driver line MB011B). Bar graphs: mean ± SEM; n = 21 – 32, for controls: n = 61. Kruskal-
1298 Wallis followed by Dunn's test ($p < 0.05$), * = $p < 0.05$.

1299 **e)** RNAi knock-down of the α5 subunit in M4/6 MBONs (driver line VT1211-Gal4) is
1300 suppressed during development using $Gal80^{ts}$. 3-5 days before the experiment RNAi-knock-
1301 down was induced. Immediate memory is significantly impaired. Bar graphs: mean ± SEM;
1302 n = 6 – 7; Kruskal-Wallis followed by Dunn's test ($p < 0.05$), * = $p < 0.05$.

1303 **f)** RNAi knock-down of the α2 subunit in M4/6 MBONs (driver line VT1211-Gal4) is
1304 suppressed during development using $Gal80^{ts}$. 3-5 days before the experiment RNAi knock-
1305 down was induced. 3-hour memories are significantly impaired. Bar graphs: mean ± SEM; n =
1306 16 – 17; one-way ANOVA followed by Tukey's test ($p < 0.05$), * = $p < 0.05$.

1307 **g)** RNAi knock-down of the α5 subunit in M4/6 MBONs (driver line VT1211-Gal4) is
1308 suppressed during development using $Gal80^{ts}$. 3-5 days before the experiment RNAi knock-
1309 down was induced. 3-hour memories are significantly impaired. Bar graphs: mean ± SEM; n =
1310 25 – 27; one-way ANOVA followed by Tukey's test ($p < 0.05$), * = $p < 0.05$.

1311 **h)** RNAi knock-down of Dlg in M4/6 MBONs (driver line VT1211-Gal4) is suppressed
1312 during development using $Gal80^{ts}$. 3-5 days before the experiment RNAi knock-down was
1313 induced. 3-hour memories are significantly impaired. Bar graphs: mean ± SEM; n = 8 – 11; one-
1314 way ANOVA followed by Tukey's test ($p < 0.05$), * = $p < 0.05$.

1315 Also see Supplementary Fig. 2 for further information.

1316

1317

1318 **Figure 3**

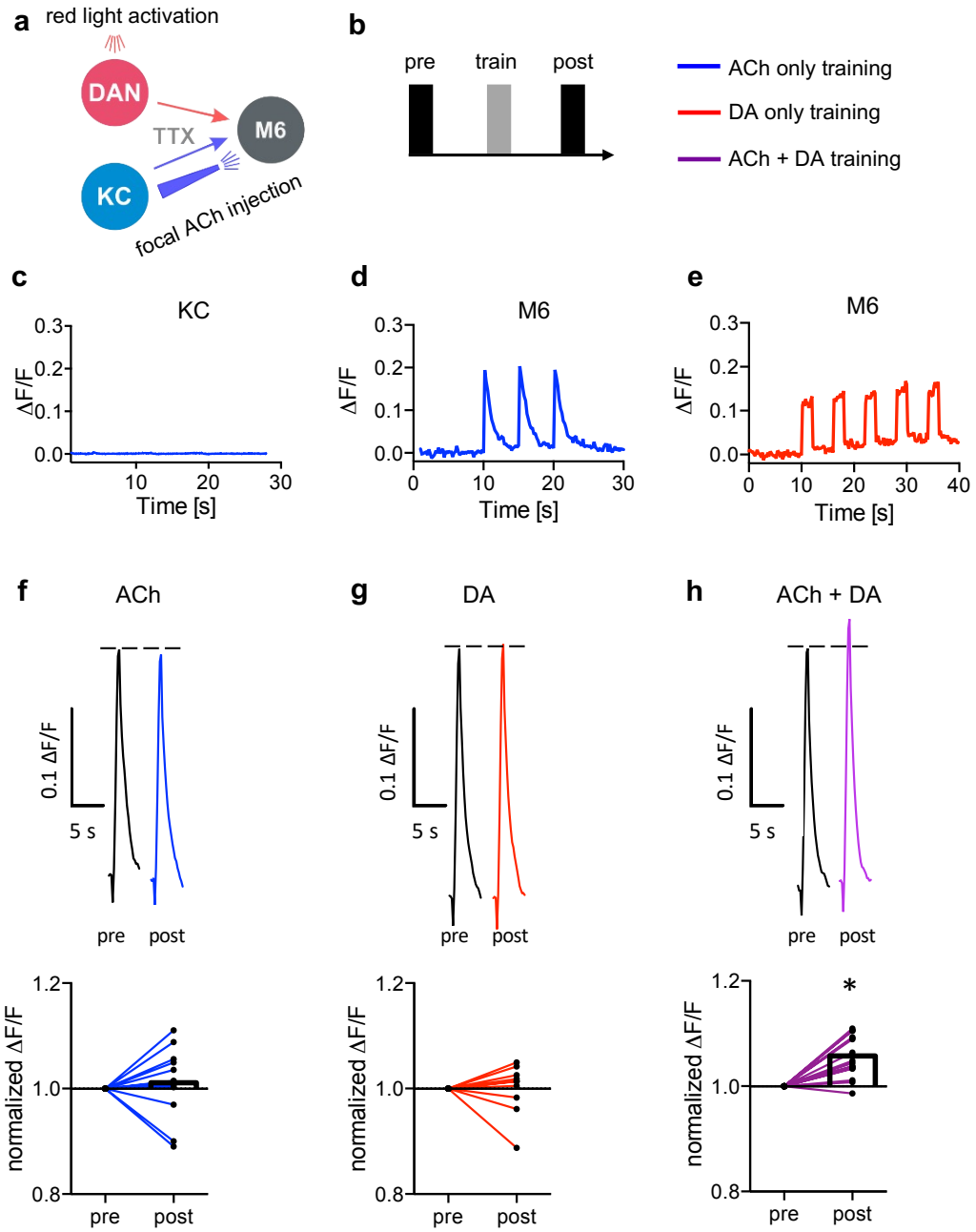

1319
1320
1321 **Figure 3: Induction of postsynaptic plasticity bypassing the presynapses.**

1322 **a)** Connectivity scheme of MB output synapses. Cholinergic KCs and dopaminergic
1323 neurons are presynaptic to M6 MBONs. Only connections relevant for this protocol are shown
1324 for simplicity. Red light pulses trigger release of dopamine (DA) from dopaminergic neurons
1325 (R58E02-LexA > lexAop-CsChrimson^{tdTomato}), while KC input is circumvented and mimicked by
1326 focal acetylcholine (ACh; 0.1 mM) injections to M6 dendrites in an explant brain preparation.
1327 Postsynaptic responses at the level of M6 are measured using GCaMP6f (MB011B > UAS-
1328 GCaMP6f). TTX in the bath suppresses feedback signaling and overall network activity within
1329 the circuit.

1330 **b)** Training scheme (top). Baseline responses to ACh application were initially established
1331 (pre). Subsequent training protocols consist of either pairing ACh application with simultaneous
1332 activation of dopaminergic neurons (purple connection lines), activation of dopaminergic

neurons (‘red light only, red connection lines), or ACh only (blue, connection lines). This is followed by a test trial (post) through ACh application.

c) Averaged traces of axonal KC calcium changes induced by focal ACh injections. No apparent transients are observable; n = 7. Line is mean ± SEM.

d) Sample trace of dendritic M6 calcium changes induced by focal ACh injections.

e) Sample trace of dendritic M6 calcium changes induced by red-light pulses.

f-h) Above: sample calcium traces in response to ACh injections recorded from M6 dendrites pre (black traces) and post (colored traces) training. Below: peak quantification.

f) Changes in acetylcholine-evoked calcium transients; comparison of mean peaks pre- and post ‘ACh only’ training. Before-after plots and bar graphs (mean); n = 13, ratio paired t-test.

g) Changes in acetylcholine-evoked calcium transients; comparison of mean peaks pre- and post ‘red light only’ training. Before-after plots and bar graphs (mean); n = 10, ratio paired t-test.

h) Changes in acetylcholine-evoked calcium transients; comparison of mean peaks pre- and post ‘paired’ training. Before-after plots and bar graphs (mean); n = 18, ratio paired t-test, * = $p < 0.05$.

Also see Supplementary Fig. 3 for further information

1351 **Figure 4**

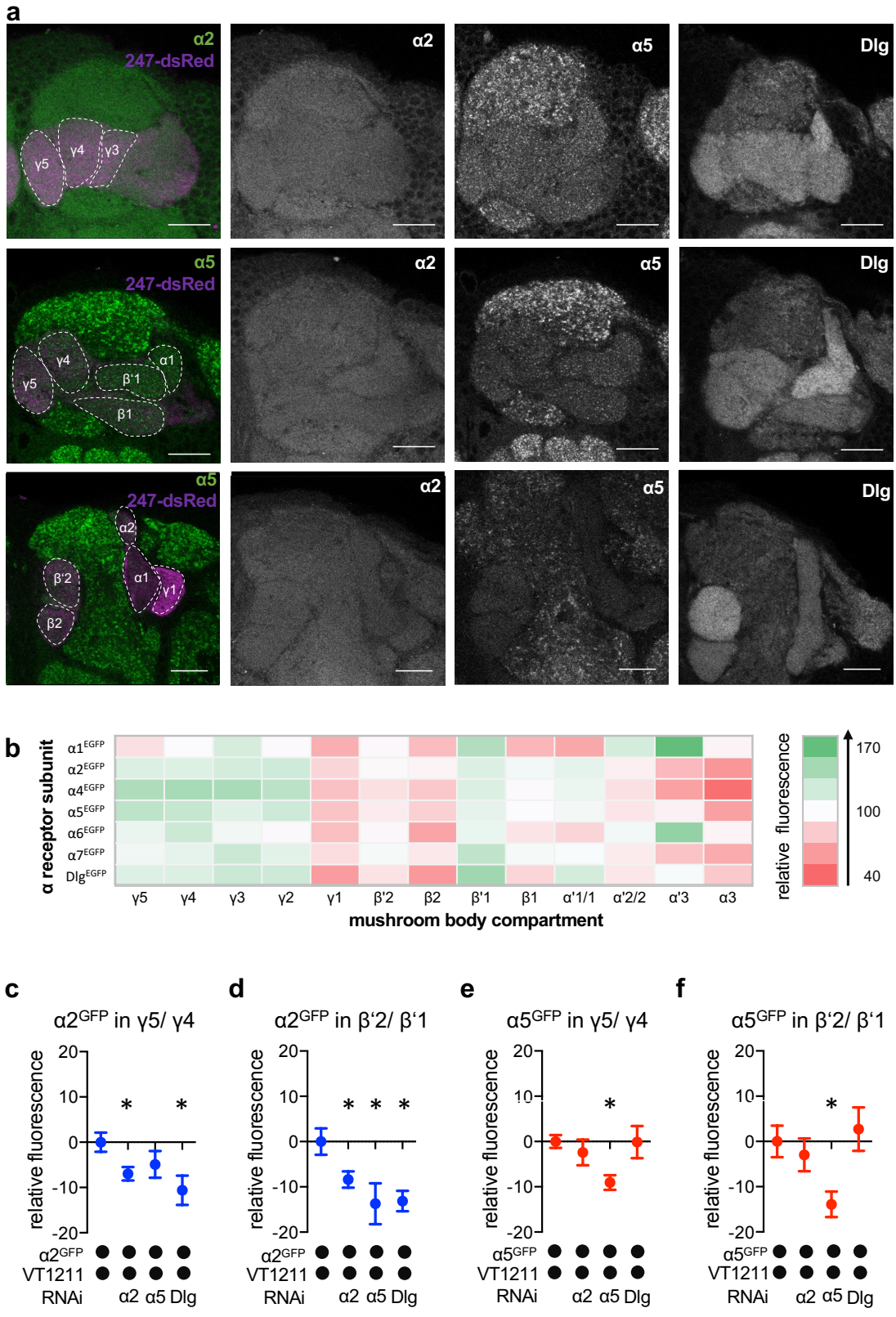

1352

1353

1354

Figure 4: nAChR α subunit localization throughout the MB: MBON-specific RNAi alters subunit distribution.

a) Representative images of the GFP-tagged nAChR subunits α2 and α5 as well as Dlg. Individual images displayed here are taken from different animals. For other subunits see Supplementary Fig. 4. Scale-Bar: 20 µm. Left: merge of α subunit signal (green) with MB compartments marked with 247-dsRed (magenta). Compartments are indicated by dashed-lines. Top row: γ compartments; middle row: α, β', β and γ compartments, bottom row: α', α and β compartments.

b) Quantification of all GFP-tagged α receptors (except for the α3 subunit). GFP signals for the indicated MB compartments are relative to the mean intensity of the GFP signal of the complete MB; n = 7 – 18.

c) Knock-down of Dlg or α2 in M4/6 neurons (driver line VT1211-Gal4) significantly reduces the $\alpha2^{GFP}$ fluorescence within the γ5 compartment (relative to unmanipulated γ4). Bar graph: normalized mean ± SEM; n = 8 – 20; Kruskal-Wallis followed by Dunn's test ($p < 0.05$), * = $p < 0.05$.

d) Knock-down of either the α2 or the α5 nAChR subunit or Dlg in M4/6 neurons (driver line VT1211-Gal4) decreases the relative fluorescence signal of $\alpha2^{GFP}$ in the β'2 compartment (relative to unmanipulated β'1). Bar graph: normalized mean ± SEM; n = 9 – 20; one-way ANOVA followed by Dunnett's test ($p < 0.05$), * = $p < 0.05$.

e) Knock-down of α5 in M4/6 neurons (driver line VT1211-Gal4) decreases the $\alpha5^{GFP}$ signal in the γ5 compartment (relative to unmanipulated γ4). Bar graph: normalized mean ± SEM; n = 9 –28; Kruskal-Wallis followed by Dunn's test ($p < 0.05$), * = $p < 0.05$.

f) $\alpha5^{GFP}$ fluorescence is significantly decreased in the β'2 compartment (relative to unmanipulated β'1) after knock-down of α5 in M4/6 neurons (driver line VT1211-Gal4). Bar graph: normalized mean ± SEM; n = 10 – 28; Kruskal-Wallis followed by Dunn's test ($p < 0.05$), * = $p < 0.05$.

Also see Supplementary Fig. 4 for further information.

1382 **Figure 5**

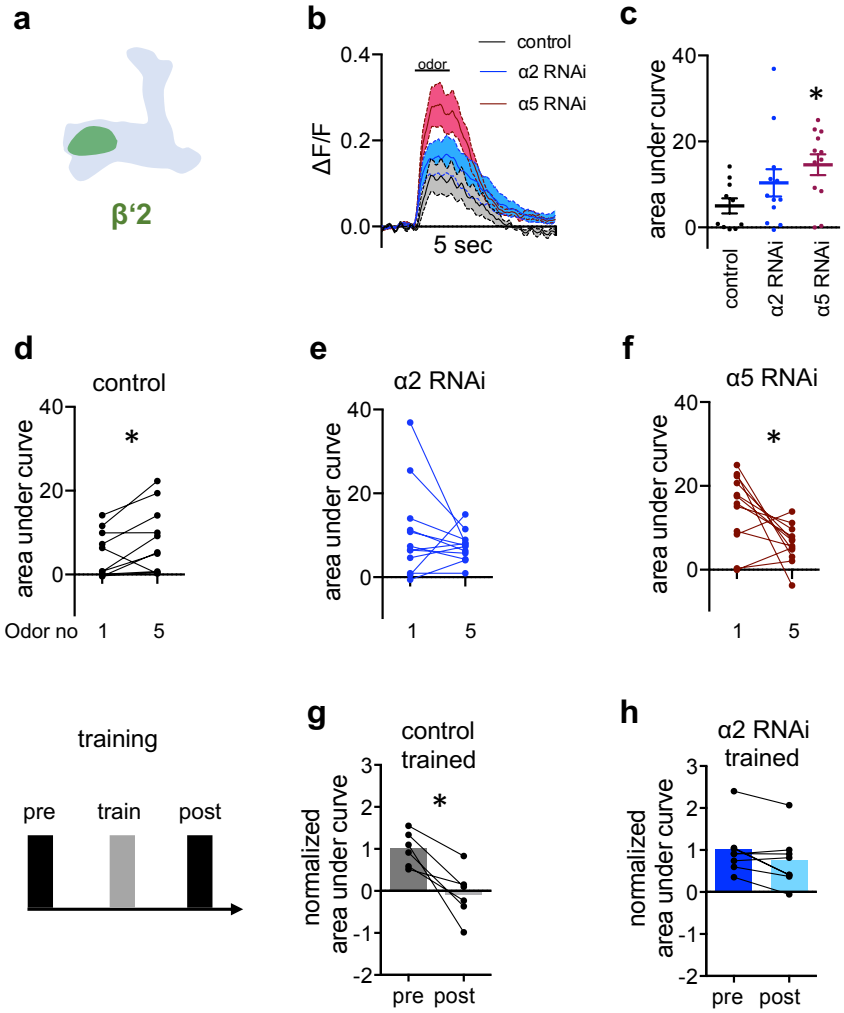

1383

1384 **Figure 5: α2 is required for learning-associated plasticity *in vivo*.**

1385 **a)** Scheme indicating the dendritic imaging area **(b-f)** at the level of the β'2 compartment.

1386 **b)** Averaged traces of GCaMP6f responses to OCT from control (black), α2 subunit RNAi
1387 (blue) and α5 subunit RNAi (red; driven in M4/6 respectively; VT1211-Gal4 as driver line) flies.
1388 Solid traces are mean, shaded areas SEM; n = 10 – 12. Odor exposure is indicated by bar.

1389 **c)** Area under curve quantifications of averaged odor responses show significantly
1390 elevated odor responses to OCT following α5 knock-down in M4/6 neurons (driver line VT1211-
1391 Gal4). Mean ± SEM; n = 10 – 12; Kruskal-Wallis followed by Dunn's test ($p < 0.05$); * = $p <$
1392 0.05.

1393 **d)** Control flies show a significant increase between the first and the fifth response to OCT.
1394 Before-after plots; n = 10; paired t-test; * = $p < 0.05$.

1395 **e)** α2 RNAi flies show no difference between the first and fifth odor response to OCT.
1396 nAChR subunit RNAi is driven in M4/6 neurons (driver line VT1211-Gal4). Before-after plots; n
1397 = 12; Wilcoxon matched-pairs signed rank test.

1398 **f)** α5 RNAi flies show a significant decrease in calcium transients over the course of
1399 consecutive odor exposures. nAChR subunit RNAi is driven in M4/6 neurons (driver line
1400 VT1211-Gal4). Before-after plots; n = 12; paired t-test; * = $p < 0.05$.

1401 **g)** Control flies show a significant decrease in GCaMP6f responses to MCH (trained odor)
1402 following absolute training (axonal imaging). Before-after plots and bar graphs (mean); n = 6;
1403 Wilcoxon matched-pairs signed rank test; * = $p < 0.05$.

1404 **h)** α2 RNAi flies show no significant decrease in GCaMP6f response to MCH (trained
1405 odor) following absolute training (driver line VT1211-Gal4, axonal imaging). Before-after plots
1406 and bar graphs (mean); n = 8; Wilcoxon matched-pairs signed rank test.

1407 Also see Supplementary Fig. 5 for further information.

1408 **Figure 6**

1409

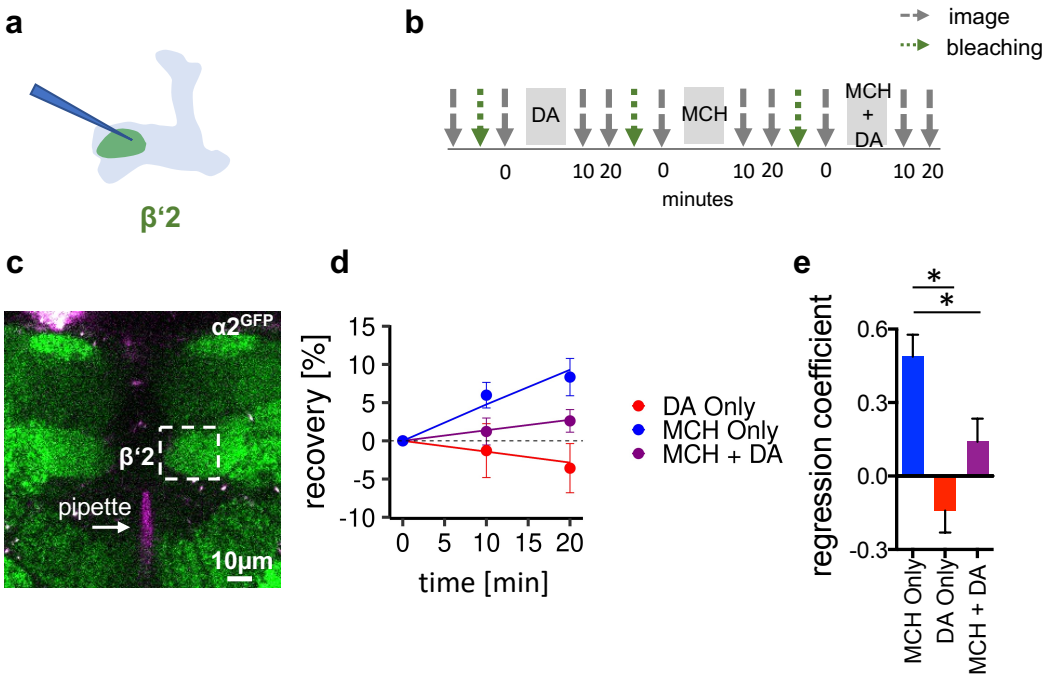

1410

1411 **Figure 6: α2 nAChR subunits dynamically rearrange.**

1412 **a**) Scheme of site of dopamine injection during fluorescence recovery after
1413 photobleaching (FRAP) experiments at the level of the KC-MBON synapses of the β'2
1414 compartment.

1415 **b)** FRAP experimental protocol. After bleaching the baseline picture was taken followed
1416 by dopamine injection, odor presentation and odor presentation simultaneously with dopamine
1417 injection in the same fly. Fluorescence recovery was monitored at the 10- and 20-minute time
1418 points.

1419 **c)** Example image of $\alpha 2^{GFP}$ expression; white dashed box shows the β'2 output zone;
1420 dopamine injection pipette (with Texas Red) is labelled in magenta. Scale bar: 10 µM.

1421 **d)** Regression of fluorescence recovery after photobleaching following MCH exposure
1422 (blue line), MCH exposure simultaneously with dopamine (DA) injection (purple line), dopamine
1423 injection alone (red line).

1424 **e)** Regression coefficient. Bar graphs: regression coefficients of recovery kinetics ±
1425 standard error of regression; n = 9 – 10, linear mixed effects model followed by pairwise
1426 comparison from estimated marginal trends. * = $p < 0.05$.

1427 Also see Supplementary Fig. 6 for further experiments.

1428

1429

1430

1431 **Figure 7**

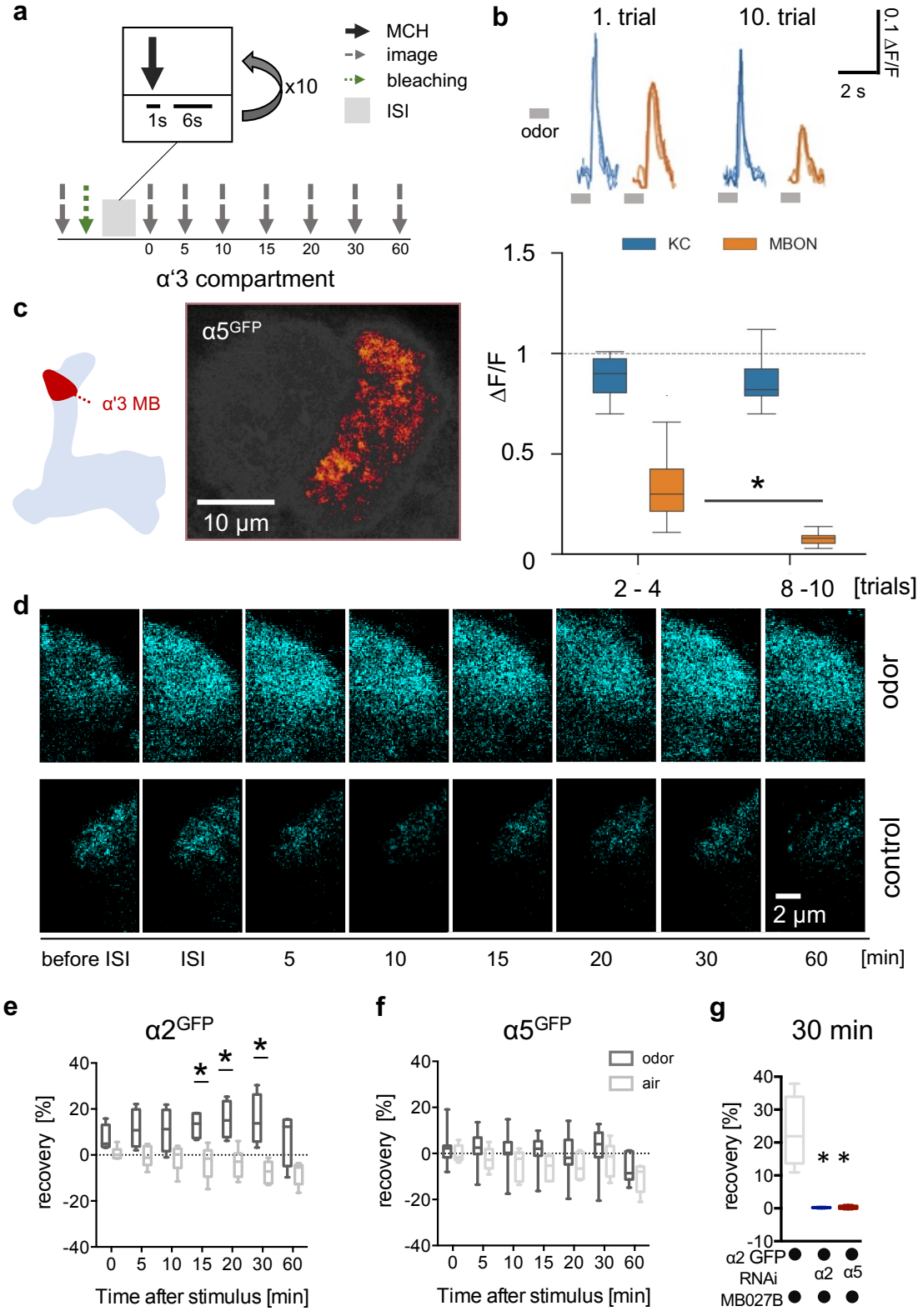

1432

1433

1434 **Figure 7: Non-associative plasticity alters postsynaptic α2 subunit receptor dynamics.**

1435 **a)** Training scheme indicating odor application, bleaching and imaging time points. MCH
1436 was given 10 times for 1 second with a pause of 6 seconds in-between. Images were taken

after training in absence of odor immediately afterwards and 5, 10, 15, 20, 30 and 60 minutes later.

b) Top: calcium peaks in response to odor stimuli of presynaptic KCs (MB369B as driver line) and adjacent postsynaptic MBONs (driver line: MB027B). Individual calcium responses to trials 1 and 10 for MBONs (orange lines) and KCs (blue lines). Bottom: Averaged calcium responses to odor stimuli of presynaptic KCs and postsynaptic MBONs of trials 2 - 4 and 8 - 10 respectively. Responses decrease at the level of MBONs but not at the level of KCs over ten trials. Box plots are median and 75 % quartiles; n = 15; Kruskal-Wallis followed by Dunn's test ($p < 0.05$), * = $p < 0.05$.

c) Scheme of α'3 compartment analyzed and representative $\alpha5^{GFP}$ fluorescent image (smoothed). Scale bar: 10 µm.

d) Example images of $\alpha2^{GFP}$ FRAP experiment at the level of the α'3 compartment at specific time points before and after training. Top row, after training; bottom row: control settings. Scale bar: 2 µm.

e) FRAP of $\alpha2^{GFP}$ nAChR subunit in the α'3 compartment after odor presentation. $\alpha2^{GFP}$ shows significant recovery following odor training compared to the controls. Recovery rate is normalized to the baseline recorded after selective bleaching of the α'3 MB compartment. Box plots are median and 75 % quartiles; n = 4 – 6; multiple t - tests with Sidak-Bonferroni correction, * = $p < 0.05$.

f) FRAP of $\alpha5^{GFP}$ subunit in the α'3 compartment after odor presentation. $\alpha5^{GFP}$ did not show significant recovery compared to the controls. Recovery rate is normalized to the baseline recorded after selective bleaching of α'3 MB compartment. Box plots are median and 75 % quartiles; n = 5 – 7, multiple t - tests with Sidak-Bonferroni correction.

g) FRAP of $\alpha2^{GFP}$ nAChR subunit in the α'3 compartment after odor presentation and knockdown of either the α2 or α5 subunit in the α'3 MBON (driver line MB027B). $\alpha2^{GFP}$ shows no recovery 30 min after odor training in α2 or α5 knockdown animals compared to the controls. Recovery rate is normalized to the baseline recorded after selective bleaching of the α'3 MB compartment. Box plots are minimum value to maximum value; n = 4 – 5; Kruskal-Wallis followed by Dunn's test ($p < 0.05$), * = $p < 0.05$.

Also see Supplementary Fig. 7 for further information.

Figure 8

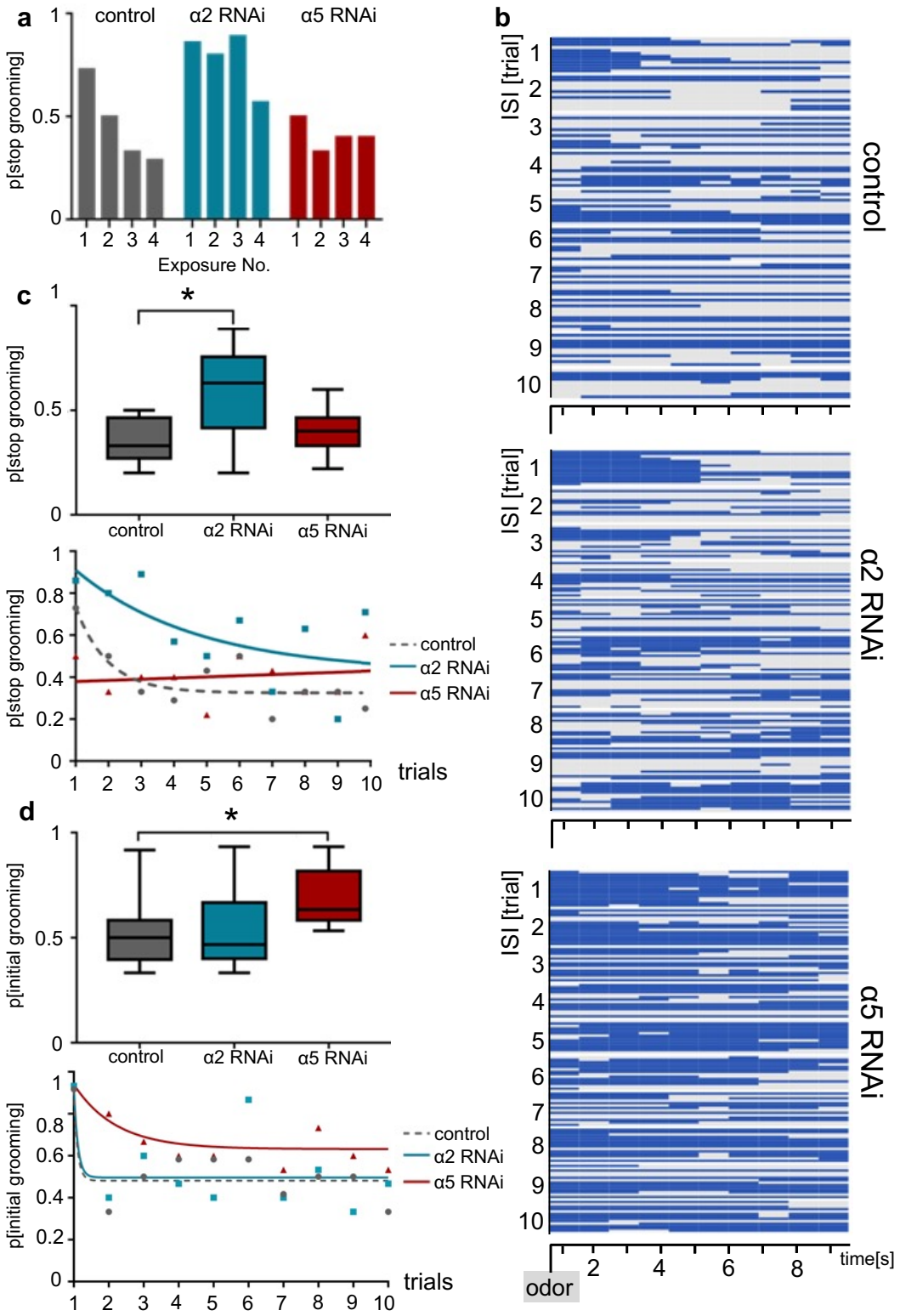

Figure 8: α2 and α5 nAChR subunits are required for non-associative familiarity learning at the level of α'3 MBONs.

a) Knock-down of α nAChR subunits at the level of α'3 MBONs alters odor familiarity learning and the probability to stop grooming. α2 RNAi knock-down delays familiarity learning effects to novel odors. α5 RNAi knock-down flies do not show a novelty response at all.

1476 **b)** Grooming behavior response of dusted flies following the repeated presentations of a
1477 novel odor (MCH). Ethogram of grooming behavior (blue) during ten intervals of odor
1478 exposures. Horizontal lines in each trial correspond to a single experimental fly within a trial
1479 group. Not grooming (grey) flies can further be categorized between pausing and wandering
1480 (see Supplementary Figure 8). n = 15.

1481 **c)** Knock-down of α2 subunit in α'3 MBONs (driver line MB027B) impairs odor familiarity
1482 learning significantly by showing a higher probability to terminate grooming responses during
1483 the learning period. The learning period is defined as the odor exposure rounds following the
1484 first exposure). Bottom graph: non-linear representation of grooming flies over ten training trials.
1485 Note that α5 behavioral responses are best described by linear representation. Box plots are
1486 median and 75 % quartiles; n = 9, one-way ANOVA followed by Dunnett's test ($p < 0.05$) * = p
1487 < 0.05.

1488 **d)** Knock-down of α5 subunits in α'3 MBONs (driver line MB027B) leads to an increased
1489 probability to start grooming earlier. 'Grooming' is defined here as constantly grooming during
1490 2 and 3 seconds after odor delivery. Bottom graph, non-linear representation of grooming flies
1491 over ten training trials. Box plots are median and 75 % quartiles; n = 9, Kruskal-Wallis followed
1492 by Dunn's test ($p < 0.05$), * = $p < 0.05$.

1493 Also see Supplementary Fig. 8 for further information.
1494

Figure 9

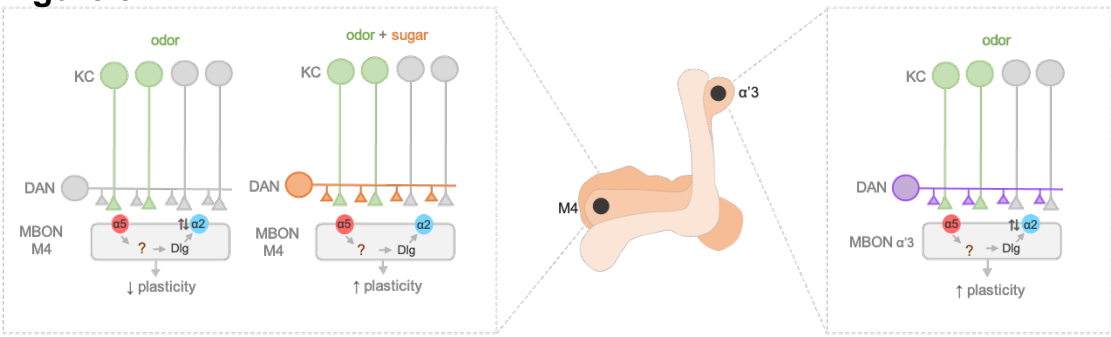

Figure 9: Model of postsynaptic plasticity sequence across compartments

Our data are consistent with a model in which α5-subunit containing receptors (red) mediate the early phase of postsynaptic memory storage, potentially by leading to elevated calcium flux (not addressed in this study) at individual postsynaptic densities (see discussion and Supplementary Fig. 9 showing separated PSDs and analyses concerning input specificity). Concurrent events see changed dynamics of the α2 receptor (blue). Nicotinic receptor subunits hereby potentially interact with adaptor proteins to bind to Dlg. Importantly, we identify elevated α2 subunit dynamics in the context of associative (M4; KC (green) and dopaminergic neuron (orange) activation needed for memory formation) and non-associative (α'3 MBONs; odor activates both KCs (green) and DANs (purple)) memory expression. Increased α2 subunit dynamics in both cases are triggered by odor application. At the level of M4, suppressed dynamics (concurrent activation of KC (green) and DAN (orange)), would correspond to postsynaptic depression, while at the level of α'3 MBONs increased dynamics could result in postsynaptic depression. Therefore, different learning rules might govern the incorporation, exchange or stabilization of receptors in or out of synapses. Please see discussion for further details.

Supplementary Information

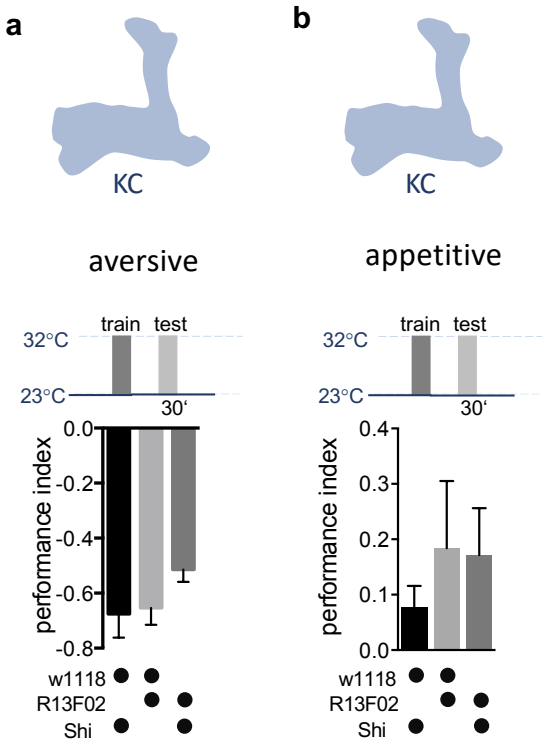

Supplementary Figure 1: Permissive temperature controls accompanying Fig. 1.

a) Permissive temperature control for experiments shown in Fig. 1a. 30 min aversive memory performance when training at 23°C (driver line R13F02-Gal4). Bar graphs: mean ± SEM; n = 7 – 9; Kruskal-Wallis followed by Dunn's test (p = 0.08).

b) Permissive temperature control for experiments shown in Fig. 1b. 30 min appetitive memory performance when training at 23°C (driver line R13F02-Gal4). Bar graphs: mean ± SEM; n = 6 – 8; Kruskal-Wallis followed by Dunn's test (p = 0.7).

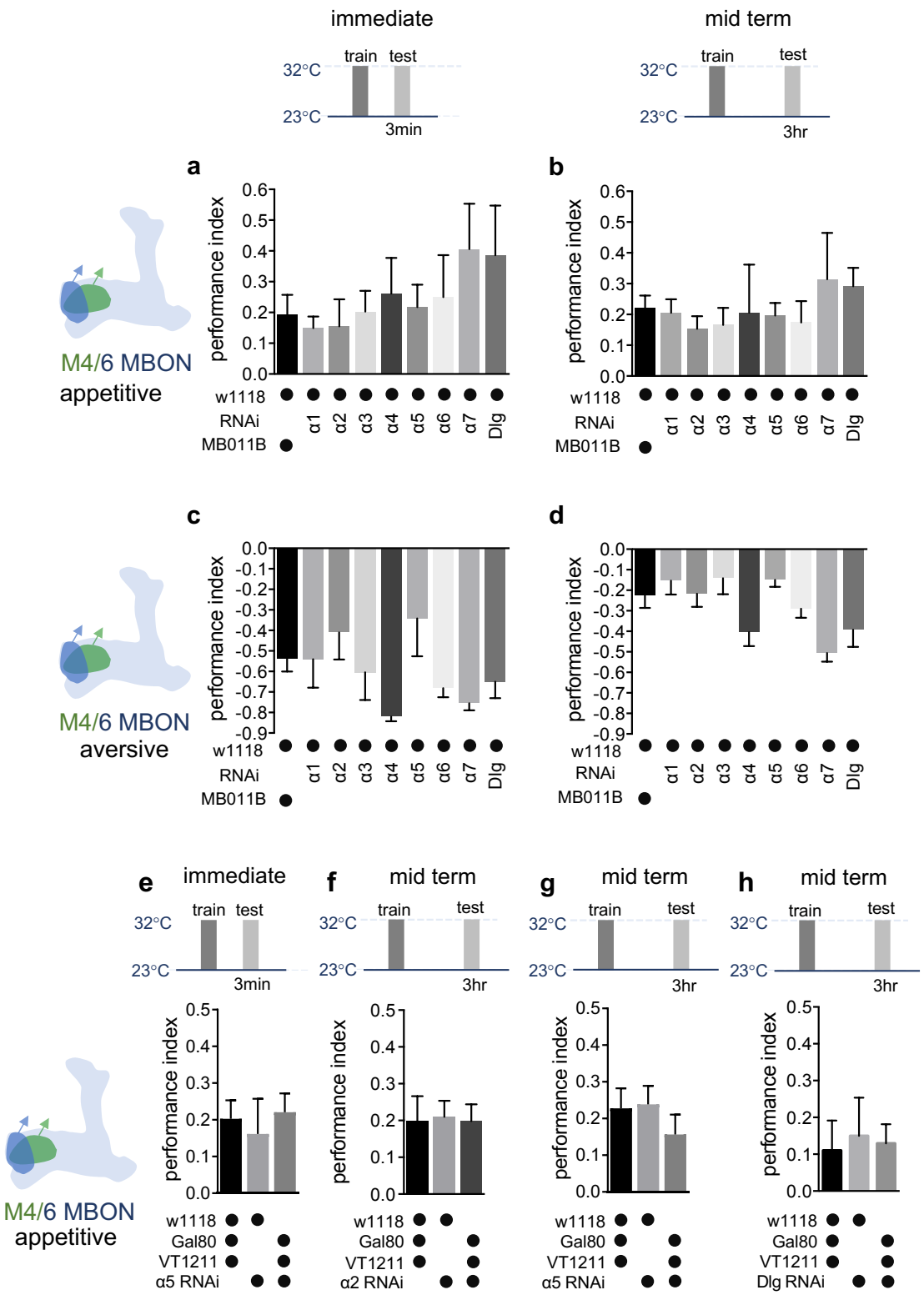
immediate
mid term
train
test
32°C
23°C
3min
3hr
a
b
c
d
e
f
g
h
performance index
M4/6 MBON
appetitive
aversive
w1118
RNAi
MB011B
α1
α2
α3
α4
α5
α6
α7
Dlg
Gal80
VT1211
α5 RNAi
α2 RNAi
Dlg RNAi

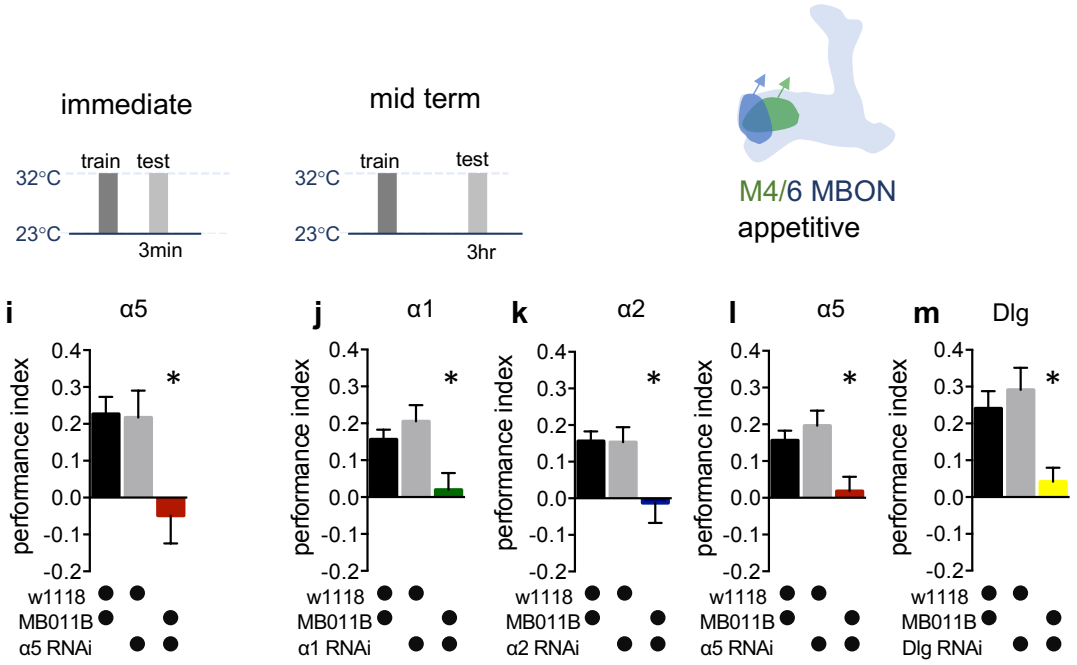

Supplementary Figure 2: Genetic controls and alternate data display of data presented in Fig. 2.

a) Immediate appetitive memory is not impaired in genetic control groups. Bar graphs: mean ± SEM; n = 7 – 11, for controls: n = 16, one-way ANOVA followed by Tukey's test ($p > 0.05$).

b) 3-hour appetitive memory is not impaired in genetic control groups. Bar graphs: mean ± SEM; n = 7 – 33, for controls: n = 41, one-way ANOVA followed by Tukey's test ($p > 0.05$).

c) Immediate aversive learning is not impaired in genetic control groups. Bar graphs: mean ± SEM; n = 6 – 10, for controls: n = 13, Kruskal-Wallis followed by Dunn's test ($p > 0.05$).

d) 3-hour aversive memory is not impaired in genetic control groups. Bar graphs: mean ± SEM; n = 6 – 10, for controls: n = 15, Kruskal-Wallis followed by Dunn's test ($p > 0.05$).

e) RNAi knock-down of the α5 subunit in M4/6 MBONs (driver line VT1211-Gal4) is suppressed using Gal80^{ts}. Immediate memories is not impaired. Bar graphs: mean ± SEM; n = 9; one-way ANOVA followed by Tukey's test.

f) RNAi knock-down of the α2 subunit in M4/6 MBONs (driver line VT1211-Gal4) is suppressed using Gal80ts. Mid term memory is not impaired. Bar graphs: mean ± SEM; n = 9 – 11, one-way ANOVA followed by Tukey's test.

g) RNAi knock-down of the α5 subunit in M4/6 MBONs (driver line VT1211-Gal4) is suppressed using Gal80ts. Mid term memory is not impaired. Bar graphs: mean ± SEM; n = 10 – 11, one-way ANOVA followed by Tukey's test.

h) RNAi knock-down of Dlg in M4/6 MBONs (driver line VT1211-Gal4) is suppressed using Gal80ts. Mid term memory is not impaired. Bar graphs: mean ± SEM; n = 8 –10, one-way ANOVA followed by Tukey's test.

(**i-m**) Alternate display (see Methods for details) for appetitive memory experiments shown in Fig. 2a,b:

i) Immediate appetitive memories are impaired following RNAi knock-down of the α5 nAChR subunit in M4/6 MBONs (driver line MB011B). Bar graphs: mean ± SEM; n = 9 – 21, one-way ANOVA followed by Tukey's test ($p < 0.05$), * = $p < 0.05$.

1569 **j)** 3-hour appetitive learning is impaired by RNAi knock-down of the α1 nAChR subunit in
1570 M4/6 MBONs (driver line MB011B). Bar graphs: mean ± SEM; n = 25 – 51, Kruskal-Wallis
1571 followed by Dunn's test ($p < 0.05$), * = $p < 0.05$.

1572 **k)** RNAi knock-down of the α2 nAChR subunit in M4/6 MBONs (driver line MB011B)
1573 impairs 3-hour appetitive memories. Bar graphs: mean ± SEM; n = 27 – 51, Kruskal-Wallis
1574 followed by Dunn's test ($p < 0.05$), * = $p < 0.05$.

1575 **l)** 3-hour appetitive learning is impaired by RNAi knock-down of the α5 nAChR subunit in
1576 M4/6 MBONs (driver line MB011B). Bar graphs: mean ± SEM; n = 27 – 51, one-way ANOVA
1577 followed by Tukey's test ($p < 0.05$), * = $p < 0.05$.

1578 **m)** RNAi knock-down of Dlg in M4/6 MBONs (driver line MB011B) impairs 3-hour
1579 appetitive memories. Bar graphs: mean ± SEM, n = 13 – 31; one-way ANOVA followed by
1580 Tukey's test ($p < 0.05$), * = $p < 0.05$.

1581

1582 Note that data in panels a-b and i-m were replotted to allow comparison between all genotypes.

1583

1584
1585
1586
1587
1588
1589

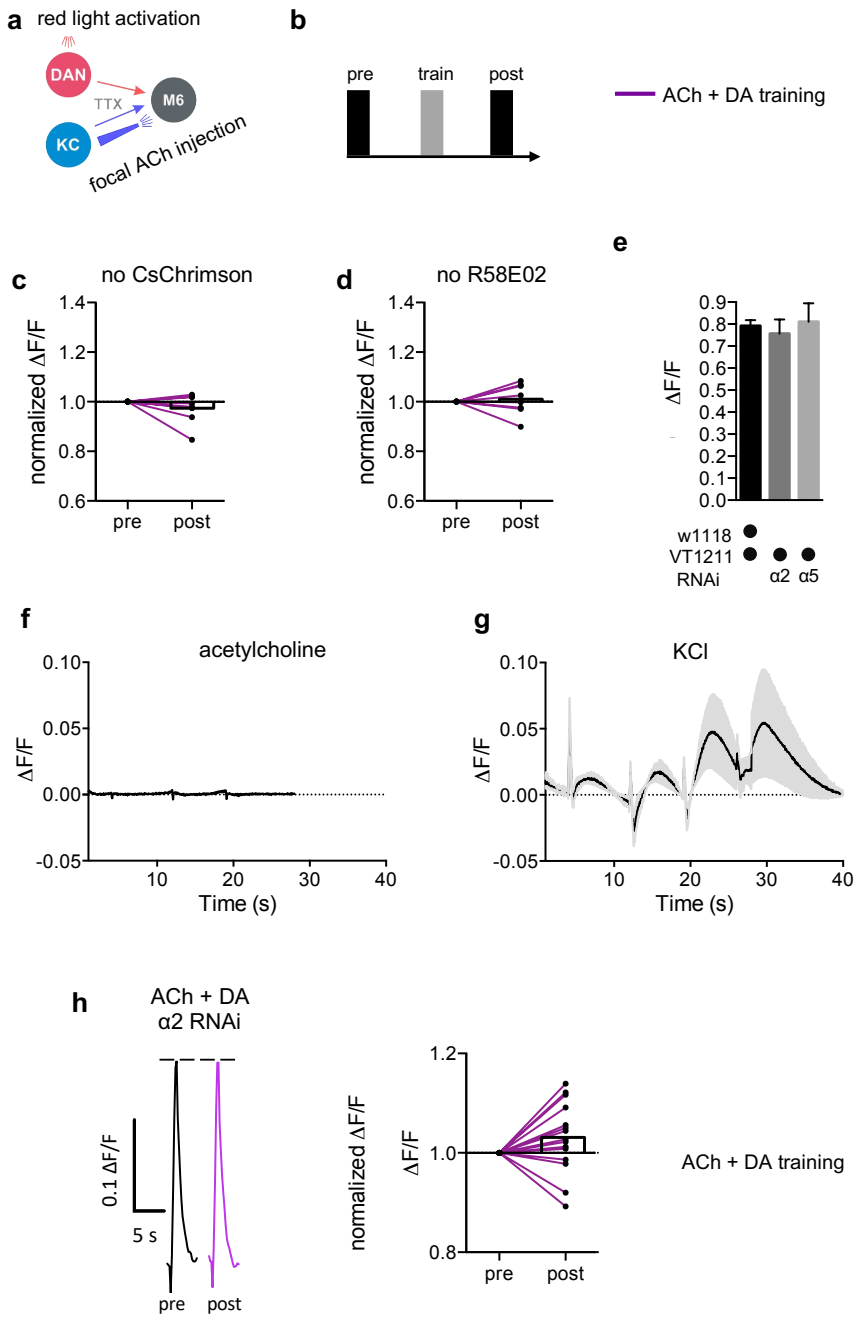

Supplementary Figure 3: Control experiments and non-normalized data display for Fig. 3.

a) Connectivity scheme of MB output synapses. Also shown in Fig. 3.

b) Training scheme.

c) Control experiments for Fig. 3 f-h. Paired training protocol in the absence of LexAoP-CsChrimson. Before-after plots and bar graphs (mean); n = 9, ratio paired t-test.

d) Control experiments for Fig. 3 f-h. Paired training protocol in the absence of R58E02-LexA. Before-after plots and bar graphs (mean); n = 8, Wilcoxon matched-pairs signed rank test.

1601 **e)** GCaMP6f responses following focal ACh injections to the γ5 compartment of the MB
1602 are not significantly altered following α2 or α5 knock-down in the M4/6 MBONs (driver line
1603 VT1211-Gal4). The bath contains TTX to suppress spontaneous neural activity. Bar graphs:
1604 mean ± SEM; n = 12 – 23, one-way ANOVA followed by Dunnett's test ($p > 0.05$).

1605 **f)** Averaged SynaptopHluorin responses following focal ACh injections (0.1 mM) to the
1606 γ5 compartment of the MB using the OK107-Gal4 driver (KCs), n = 8. Shaded area depicts
1607 SEM.

1608 **g)** Averaged SynaptpHluorin responses following focal KCl injections (300-400 mM) to the
1609 γ5 compartment of the MB using the OK107-Gal4 driver (KCs), n = 4. Shaded area depicts
1610 SEM.

1611

1612 **h)** Left: sample calcium traces in response to ACh injections recorded from M6 dendrites
1613 pre (black traces) and post (colored traces) training. Right: peak quantification.
1614 Following RNAi knock-down of the α2 subunit in M4/6 MBONs no significant potentiation was
1615 detected after paired acetylcholine application and dopaminergic neuron activation. Before-
1616 after plots and bar graphs (mean); n = 15, ratio paired t-test.

1617

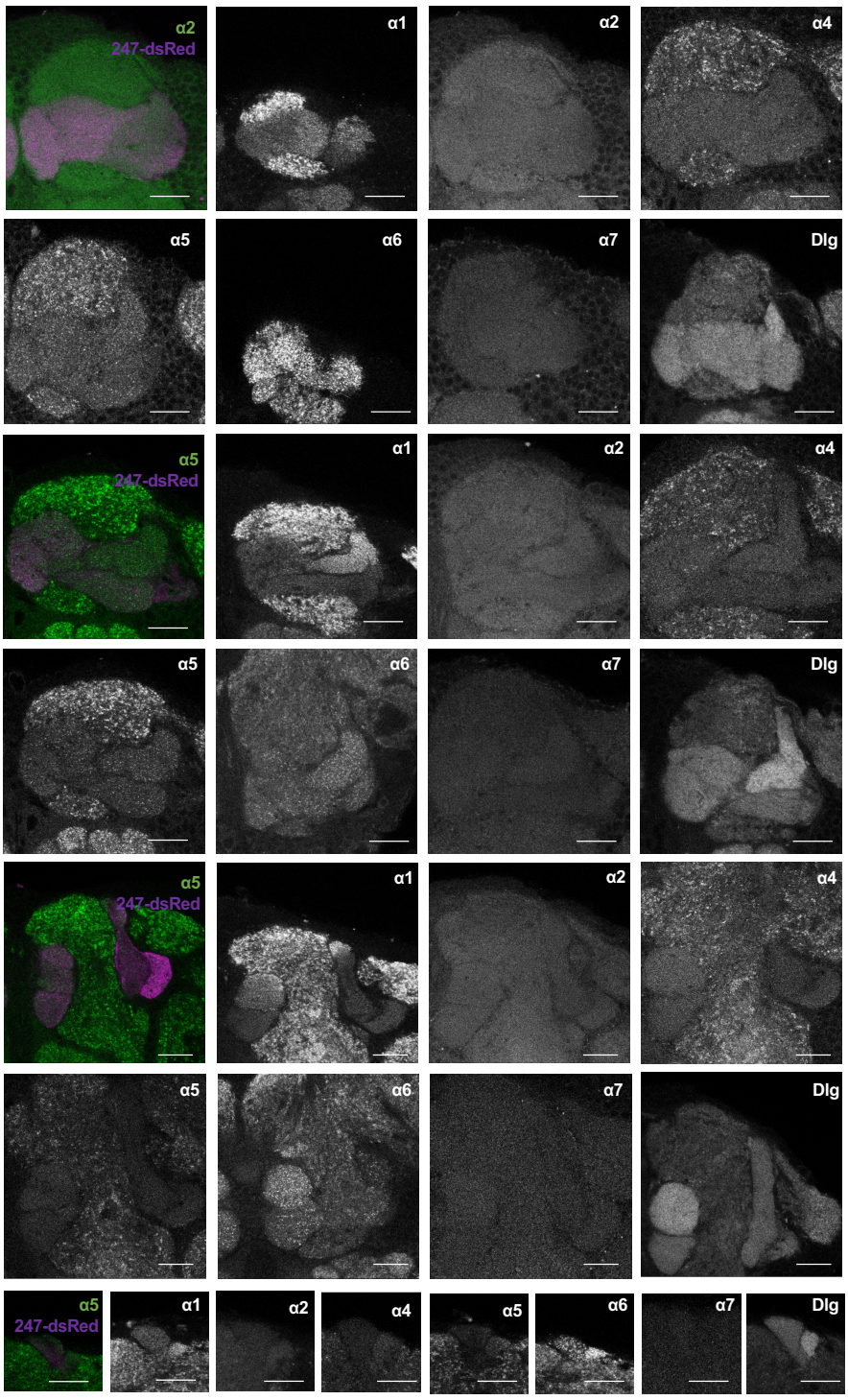

Supplementary Figure 4: Detailed distribution of α subunits in the MB accompanying Fig. 4.

Example image planes of GFP expression at the level of the MB compartments for all α nAChR subunits (except for α3) and Dlg. Pictures are taken from different animals. Scale-Bar: 20 µm. Left: merged image of α subunit signal (green) with MB compartments marked by 247-dsRed (magenta). Top two rows: γ compartments; middle two rows: γ, β' and β compartments, bottom three rows: α'/β' and α/β, with bottom row: α' and α compartments.

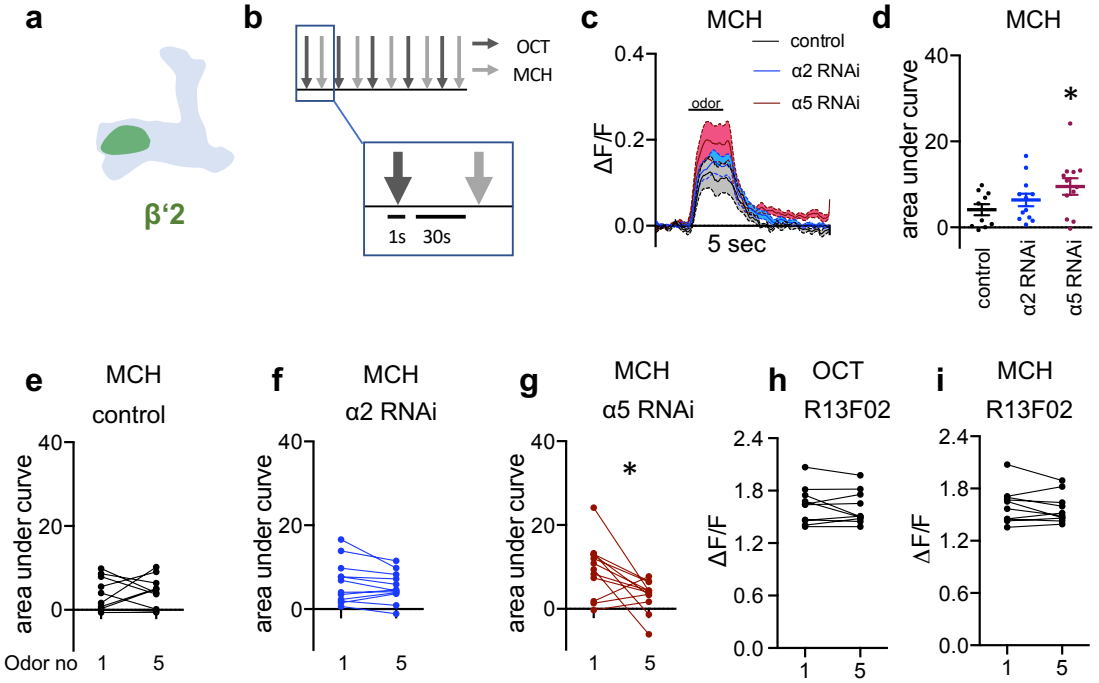

Supplementary Figure 5: Additional data and display of non-normalized data accompanying Fig. 5.

a) Scheme indicating the imaging area at the level of the β'2 compartment.

b) Odor exposure protocol. 5 OCT stimuli were alternatingly administered with 5 MCH stimuli. 1 second odor puffs were separated by 30 seconds breaks. Odor responses are measured using GCaMP6f as in Fig. 5.

c) Averaged traces of GCaMP6f (calcium) responses to MCH from control (black), α2 (blue) and α5 RNAi (red; driven in M4/6 respectively, driver line VT1211-Gal4) flies. Solid traces are mean, shaded areas SEM; n = 10 - 12. Odor exposure is indicated by bar.

d) Area under curve quantification of averaged odor responses show significantly elevated odor responses to MCH following α5 knock-down in M4/6 neurons (driver line VT1211-Gal4). Mean ± SEM; one-way ANOVA followed by Dunnett's test ($p < 0.08$), * = $p < 0.05$; n = 10 – 12.

e) Control flies show no significant increase between the first and the fifth response to MCH. n = 10; paired t-test.

f) α2 RNAi flies show no difference between the first and fifth odor response to MCH. nAChR subunit RNAi is driven in M4/6 neurons (driver line VT1211-Gal4). n = 12; paired t- test.

g) α5 RNAi flies show a significant decrease in calcium transients over the course of consecutive odor exposures. nAChR subunit RNAi is driven in M4/6 neurons (driver line VT1211-Gal4). n = 12; Wilcoxon matched-pairs signed rank test; * = $p < 0.05$.

h) KCs (driver line R13F02-Gal4) show no significant change in calcium transients over the consecutive OCT odor exposures. Before-after plots. n = 10, paired t- test.

i) KCs (driver line R13F02-Gal4) show no significant change in calcium transients over the consecutive MCH odor exposures. Before-after plots. n = 10, paired t- test.

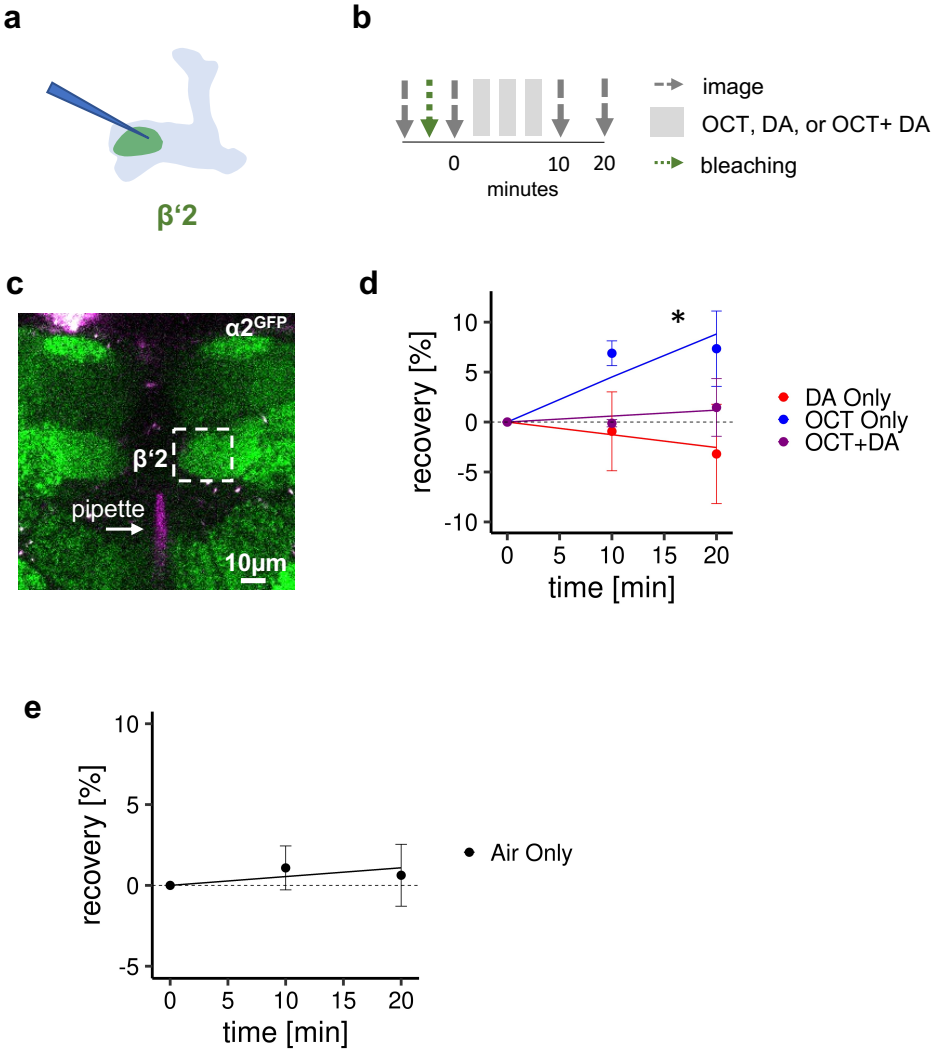

Supplementary Figure 6: Receptor subunit recovery, accompanying Fig. 6.

a) Scheme of site of dopamine injection during fluorescence recovery after photobleaching (FRAP) experiments at the level of the KC-MBON synapses of the β'2 compartment.

b) FRAP experimental protocol. After bleaching, a baseline picture was taken followed by odor presentation or odor presentation simultaneously with dopamine injection or dopamine injection by itself. Fluorescence recovery was monitored at the 10 and 20 minute time points.

c) Example image of $\alpha2^{GFP}$ expression (the same image is shown here as in Fig. 6); white dashed box shows the β'2 output zone; dopamine injection pipette (with Texas Red) is labelled in magenta. Scale bar: 10 µm.

d) Regression of fluorescence recovery after photobleaching following OCT exposure (blue line), or OCT exposure simultaneously with dopamine (DA) injection (purple line), or dopamine injection alone (red line). n = 3 –5, t-test, Satterthwaite's method for approximating the degrees of freedom. *: regression coefficient $p < 0.05$ in the linear mixed effect model. Only 'OCT only' exposure shows recovery that significantly differs from 0.

e) Control settings for Fig. 6 and the experiments shown in this figure. After bleaching, $\alpha2^{GFP}$ flies were exposed to air only. n = 9, t-test, Satterthwaite's method for approximating the

degrees of freedom. The regression coefficient is not significantly different from 0.

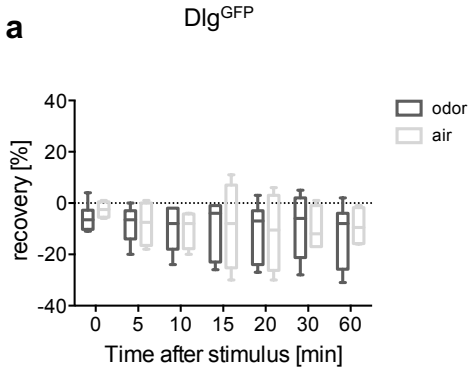

Supplementary Figure 7: Dlg^{GFP} FRAP, accompanying Fig. 7

a) FRAP of Dlg^{GFP} in α'3 MBONs. Dlg^{GFP} did not show significant recovery. Recovery rate is normalized to the baseline recorded after selective bleaching of the α'3 MB compartment. n = 5 - 7; multiple t-tests.

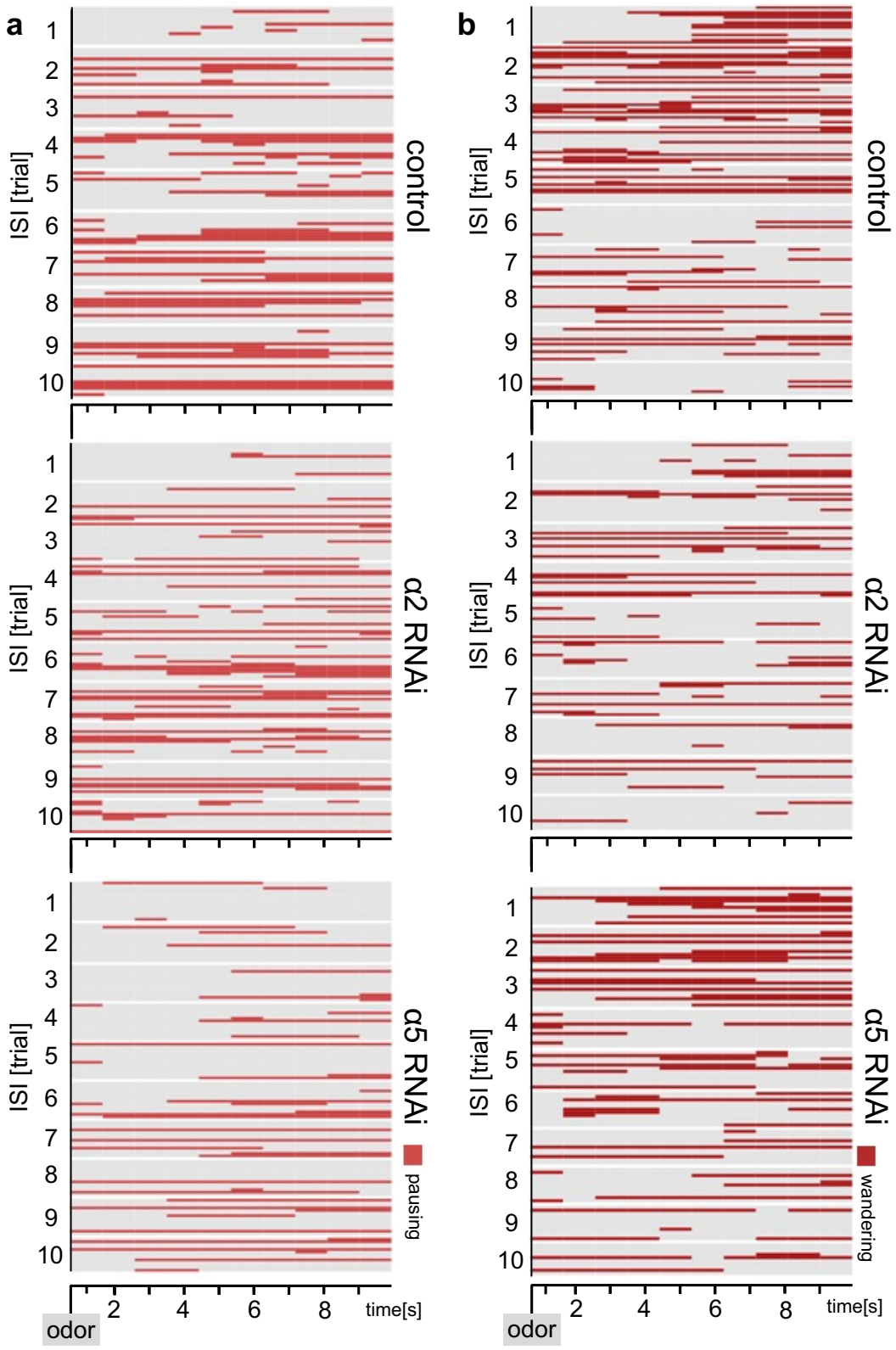

Supplementary Figure 8: Additional ethograms, accompanying Fig. 8.

a, b) Ethograms of the behavioral responses of flies shown in Fig. 8 with additional behavioral categories of pausing and wandering (when not grooming). Ethograms show pausing (red, **a**) which is defined as not moving and not grooming or wandering (dark red, **b**) which is defined as moving around in the chamber.

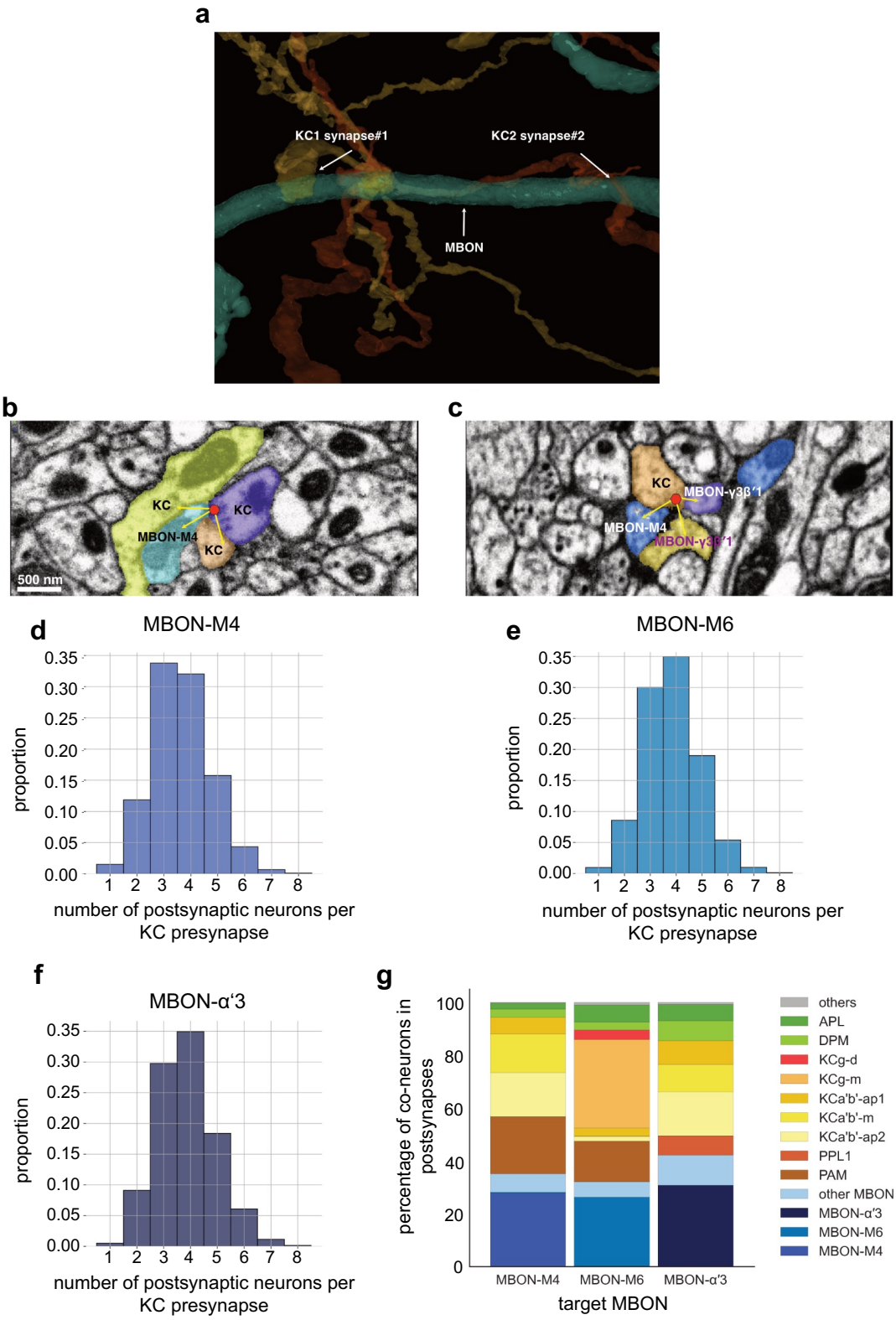

Supplementary Figure 9: Input analysis of KC to MBON synapses, accompanying Fig. 9.

a) Reconstructed example synapses from electron microscopic (EM) volume (neuprint.org)[62]: two different KCs connect to the same MBON on the postsynaptic side.

b) EM image (neuprint.org) showing a KC presynapse simultaneously innervating two other KCs and the M4 MBON. Scale bar: 500 nm.

c) EM image (neuprint.org) showing a KC presynapse simultaneously innervating the M4 MBON and two sites of another MBON.

d) Analysis of number of postsynaptic partners for each KC presynapse identified providing input to M4. The histogram shows the distribution of KC synapses to M4 relative to how many postsynaptic partners the KC presynapses have.

e) Analysis of number of postsynaptic partners for each KC presynapse identified providing input to M6. The histogram shows the distribution of KC synapses to M6 relative to how many postsynaptic partners the KC presynapses have.

f) Analysis of number of postsynaptic partners for each KC presynapse identified providing input to α'3 MBONs (pooled). The histogram shows the distribution of KC synapses to α'3 MBONs relative to how many postsynaptic partners the KC presynapses have.

g) Percentage of types of neurons that share a KC presynapse with a given MBON.